Cylindrical Colloids on a Fluid Membrane

by

Sergey Mkrtchyan

A thesis
presented to the University of Waterloo
in fulfillment of the
thesis requirement for the degree of
Master of Science
in
Physics

Waterloo, Ontario, Canada, 2009

I hereby declare that I am the sole author of this thesis. This is a true copy of the thesis, including any required final revisions, as accepted by my examiners.

I understand that my thesis may be made electronically available to the public.

Abstract

We theoretically study the adhesion and membrane-mediated interaction of cylindrical colloids to a flat fluid membrane. There are two ways to approach this problem. The first way, based on energy, requires finding the equilibrium shape of the membrane given the placement of the particle(s). In order to do so, we need to know how the energy of the surface depends on its shape (i.e. the surface Hamiltonian), as well as how the adhered colloid deforms the membrane. The second way to approach this class of problems is "geometrical", where forces between the membrane-adhered particles are related directly to the geometry of the deformed membrane via the surface stress tensor. The surface Hamiltonian allows finding the stress at any point on the membrane in terms of local geometry. The force acting on the colloid can then be found by integrating this surface stress tensor along any contour enclosing the colloid.

In this thesis, using the approach based on free energy calculations, we look into the problem of cylindrical colloids adhering to a membrane with fixed constant adhesion energy between the membrane and the colloids. Angle-arclength parameterization is used in order to treat the problem beyond small gradient approximation. We present three different cases here: single cylinder adhering on a membrane, two cylinders adhering on the same side of the membrane, and two cylinders adhering on different sides of the membrane. For the single cylinder case we present a structural phase diagram to separate no wrapping, partial wrapping and closure states and we compare it to the phase diagram obtained for a related system of spherical colloids. For two cylinders adhered on the same side of the membrane we obtain repulsive interaction and transition from shallow to deep wrapping as the cylinders move apart from each other. We also look into a phase where two cylinders are vertically stacked and discuss its energetics. For two cylinders adhering to the opposite sides of the membrane, attractive interaction is obtained in accordance with previous results and we further show that in that case two cylinders are generally in contact and a first-order transition from shallow to full wrapping is possible. In the last section, we put a framework for the class of problems where the particle is between the membrane and the supporting interface, where adhesion is assumed between the interface and the membrane.

Acknowledgements

I would like to thank my supervisor, Professor Jeff Z.Y. Chen for his support and patient guidance in each step of my work on the thesis. I'm also grateful to my committee members Professors Russel B. Thompson, Robert Wickham and Bae-Yeun Ha for helpful comments and assistance.

This work was made possible by the facilities of the Shared Hierarchical Academic Research Computing Network (SHARCNET:www.sharcnet.ca).

Contents

List of Tables

List of Figures

Chapter 1

Introduction

Membranes play a crucial role in both structure and function of cells. Not only the membranes serve to divide the different space regions but they allow communication between neighboring compartments. Most significantly the communication is mediated by the passage of the ions or molecules between the compartments or by the information transmitted through conformational changes induced in membrane components [1]. Most of the fundamental biochemical functions in cells involve membranes at some point, including processes like DNA replication, protein biosynthesis, protein secretion, bioenergetics and hormonal responses.

1.1 What Are Membranes?

A membrane is a layer of material which serves as a separating barrier between two compartments in biochemical environment. Membranes can be of various thickness, but generally, for the problems we are interested in, it can be assumed that the thickness of the membrane is much smaller than its length or width, and therefore it can be represented as a two-dimensional sheet embedded in the three dimensional space.

We are interested in a biological membrane, which is a bilayer of lipid-type molecules, with occasional proteins embedded into the membrane. The basic building block of the bilayer is a lipid molecule, specifically phospholipids and cholesterol. We are not very concerned about their chemical structure, but rather that the lipid molecule is an amphiphile, meaning that it consists of two different parts: a hydrophilic head and a hydrophobic tail. In an aqueous environment, hydrophobic tails cannot form hydrogen bonds and therefore water repels them in favor of bonding with itself. However hydrophilic heads are able to form hydrogen bonds and prefer to stay in the water. This causes amphiphiles to form into aggregate structures when their concentration in aqueous solution is above the critical value. At that concentration, called *critical micelle concentration*, it becomes energetically favorable for amphiphiles to sacrifice some of their entropy and form into aggregates in order to shield their hydrophobic tails against the surrounding water by

using the hydrophilic heads. Depending on the relative size of the hydrophilic head and hydrophobic tail, the morphology of the aggregate can vary from spherical or cylindrical micelles to bilayers or vesicles. We will be interested in one-component lipid-bilayer structure shown on the figure 1.1, which is a double layer in which the hydrophobic tails are sandwiched between two planes of hydrophilic head groups.

We considered the membrane from a mesoscopic point of view assuming that lateral extension and all deformations are much larger than the thickness of the membrane.

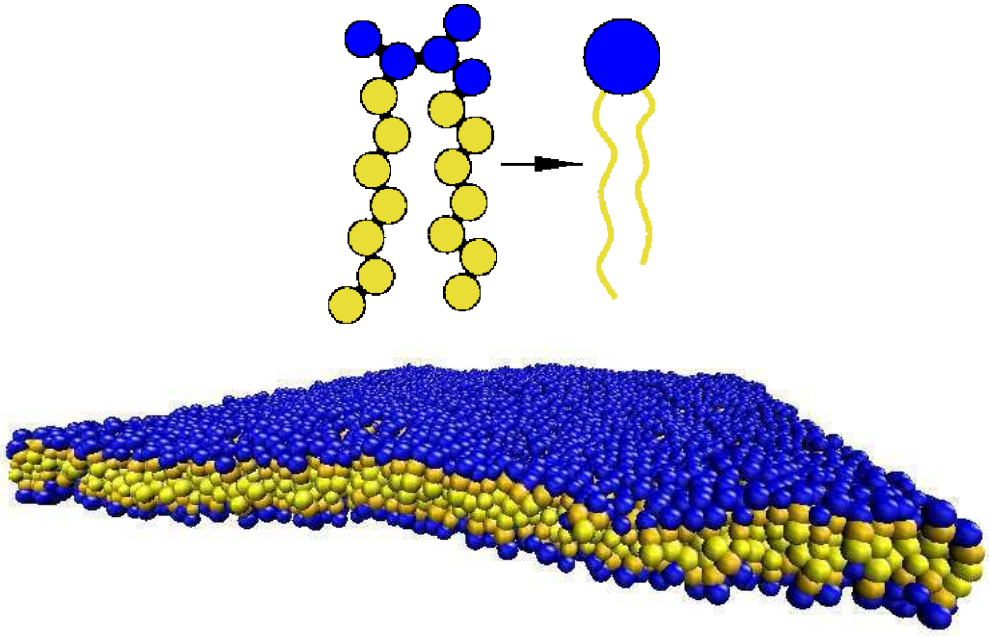

Figure 1.1: Schematic illustration of a lipid, consisting of a hydrophilic head (represented by a blue sphere) and a hydrophobic tail (shown in yellow) and illustration of a lipid bilayer model obtain by coarse-grained simulations (images are taken from references [2] and [3]).

1.2 Membrane Interaction with Colloids

Many biological processes are controlled by the interaction of macromolecules with a cell membrane. One of the most important properties of cell membranes is their ability to control transport mechanisms. The size of the particles (colloids, nanoparticles, viruses etc.) being transported can vary from angstroms, for ions such as Na^+ or Ca^{2+}, to micron-sized viral particles. For small particles the transport through the cell membrane is mediated by membrane proteins acting as transport channels [4]. For micron-sized particles however, where sizes are typically much

larger than membrane thickness, the transport mechanism for entry and exit processes is entirely different. Entry of the virus into the cell occurs through a process called membrane fusion (which occurs during endocytosis, schematically shown on Fig. 1.2) and viruses exit the cell by budding. In both processes the membrane envelops the particle that deforms the membrane on a scale much larger then its thickness. This continues until the full envelopment and subsequent pinching off of the particle [1]. Viral budding has been verified experimentally by Rhee et al. [6]

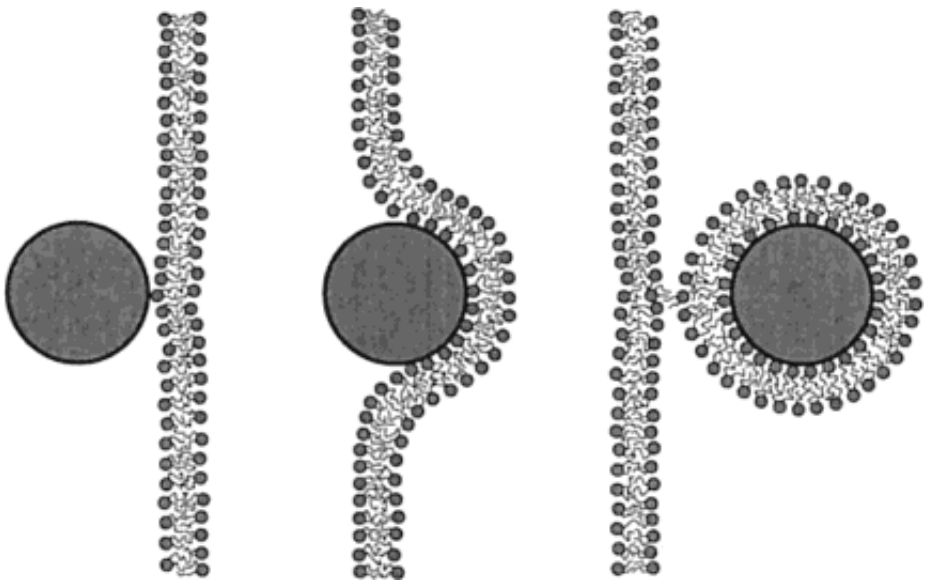

Figure 1.2: Schematic Illustration of the process of endocytosis (image taken from reference [5])

and Garoff et al. [7]

A similar transport mechanism occurs in gene transfection systems as suggested by Boussif et al. [8]. It is assumed that DNA is complexed into a globular structure, that enters the cell by adhesion. The interaction with the membrane is a result of the electrostatic attraction between the positively charged complex with the negatively charged regions of the membrane.

A great deal of experimental techniques involve the attachment of microbeads to a membrane. As an example thermodynamic aspects of the deformation and flow of the membrane into a tether has been discussed by Hochmuth et al in [9]. There thin tethers were extracted from a membrane by attaching a tether to a bead which was held in place with a force created by an optical laser trap or "tweezer". Cell surface tensions were measured by measuring different forces applied on the beads and different tether flow speeds.

Cell membranes are also probed with atomic force microscopes, where AFM tips are adhered to a membrane and then are subjected to a force [10]. As for the case with optical tweezer, here also the object adhering on a cell membrane deforms it locally, which can be crucial for interpreting experimental result.

Understanding the adhesion and consequent interaction of the adhered particles is important in nanocarrier agent design and drug delivery [11]. Flexible membranes of the vesicles in contact with nanoparticles has been studied theoretically by Lipowsky et al in [12], where it was shown that adhering particles change spontaneous curvature of the membrane, which is dependent on the membrane particle interaction type and the size of the particles. Vesicle interaction with Brownian dynamics simulation has been studied by Noguchi et al in [13], where budding, formation of two vesicles and fusion has been observed.

Membrane mediated attraction and aggregation of colloidal particles has been studied using light microscopy by Koltover et al in [14]. It has been observed that membrane deformations induce particle interaction on the range which is about the diameter of the particles. Hydrophobic/hydrophilic interaction of nanoparticles with the membrane was studied computationally by Li et al in [15], and it was observed that hydrophobicity of nanoparticles can result in inclusion into the membrane, which hydrophilic nanoparticles only adhere to a membrane.

Experimentally the system was studied by Binder et al in [16], where budding effects of large viral particles have been observed.

In all above cases it has been shown that nanoparticle adhesion on a membrane induces structural change of the membrane, which range from small to large deformations.

1.3 Previous Research

We studied the adhesion of cylindrical particles on a fluid membrane. Static and dynamic aspects of membrane and vesicle configurations of this nature have been considered in detail in [17]. The process of the adhesion of a particle to a membrane was considered as a competition between curvature energy (coming from bending elasticity of the membrane) and geometrical restraints such as fixed surface area or volume (which create an effective tension). A number of equilibrium shapes were arranged into phase diagrams, separating regions with different symmetry by continuous or discontinuous transitions.

Enforced unbinding from a supporting membrane was considered by Boulbitch in [18] for cylindrical colloids. Adhesion of cylindrical colloids onto a membrane and their subsequent membrane-induced interaction was discussed previously by Weikl in [19]. Monge parameterization was used in both cases, where the surface of the membrane was described by specifying its height h above an arbitrary horizontal reference plane. In that case, if r is the two-dimensional position-vector in that plane, the shape of the membrane will be given by $h(r)$. Monge parameterization is frequently used for studies of this nature, but it is only suitable for small membrane deformations, where no overhangs are taken into account.

For small membrane deformations, repulsive interaction was observed by Weikl in [19] between the cylinders adhered at the same side of the membrane and attrac-

tive interaction between the cylinders adhered at opposite sides. A membrane in an external harmonic potential was also considered and it was shown that in this case the interaction of adsorbed cylinders was always attractive.

A related system for spherical colloids was discussed by Deserno in [20]. In this case arclength parameterization was used, where the membrane profile was given by specifying, at any point on the membrane, the angle of the tangent with respect to horizontal as a function of arclength s. This approach is not restricted to small membrane deformations and allows the consideration of deep wrapping regions, which occur for large adhesion energies. Structural and energetic aspects of a single sphere adhering on a membrane were discussed in detail. Both continuous binding and discontinuous envelopment transitions were observed for spherical particles.

For adhered particles, in another work of Deserno [21] membrane-mediated interactions were discussed relating the forces between the particles directly to the local geometry of the membrane using balance of torques. General framework for this "geometrical" approach was proposed and the case of infinitely long cylindrical colloids was discussed in that framework. Two approaches were suggested, where in the first one, the problem was treated assuming constant area of wrapping, while for the second one constant adhesion energy was assumed. For the constant area of wrapping case, detailed results were brought, discussing the equilibrium shapes of the membrane as well as forces between the cylindrical colloids. We will concentrate on the case, where adhesion energy is constant.

We use angle-arclength parameterization used in [20] and consider the system of cylindrical colloids using the approach based on free energy calculations. We discuss single cylinder adhering on a membrane, and separate three states - no wrapping, partial wrapping and closure. We show a phase diagram separating those and compare it to the phase diagram obtained by Deserno for a system of spherical colloids. We also discuss two cylinders adhered on a membrane in both symmetric and anti-symmetric cases in a non-linear regime. In the last section, using the tools already developed we put a framework for the class of problems, where colloids are between the membrane supported on an interface.

In the above mentioned problems we assume constant adhesion energy, but in order to compare with Deserno's results in [21] we also look into the problem of two cylinders on the same side of the membrane in the constant wrapping angle scenario. We look into equilibrium shape profiles of the membrane and compare quantitatively with the results obtained by Deserno.

Chapter 2

Model and Energy Considerations

We considered the adhesion of cylindrical colloids to a fluid membrane. The size of all deformations is assumed to be much larger than the thickness of the membrane, therefore we model the membrane as a two-dimensional surface in three dimensional space.

2.1 General Model and Geometry

We model the geometry of the membrane using angle-arclength parameterization as shown in Fig. 3.1. In order to fully describe our system it is advantageous to parameterize the membrane shape by specifying the angle of the tangent with respect to the horizontal as a function of s, arclength of the curve. In that case we can take into account overhangs and generally will not be restricted to small membrane deformations. Previous work on this system implemented a more direct choice, which was to measure h, the deviation from the reference plane, as a function of coordinate perpendicular to cylinder axis [19, 18], which is useful for small-gradient approximation. This system was also discussed later on in [21] where balance of torques was imposed directly from the specific shapes of the membrane. In this thesis, we use arclength parameterization and look into the energetics of the system.

In the arclength parameterization membrane shape is given by specifying the angle ψ with respect to horizontal as a function of s, the arclength of the curve.

$$\psi = \psi(s). \tag{2.1}$$

From Fig. 3.1 we can see that it is related to the Cartesian coordinate system through the following equations

$$\dot{x} = \cos\psi \text{ and } \dot{y} = \sin\psi, \tag{2.2}$$

where by dot we indicate the derivative with respect to the arclength s. We can write it alternatively in the form

$$dx = \cos\psi ds = \cos\psi \frac{ds}{d\psi} d\psi = \frac{\cos\psi}{d\psi/ds} d\psi, \tag{2.3}$$

$$dy = \sin\psi ds = \sin\psi \frac{ds}{d\psi} d\psi = \frac{\sin\psi}{d\psi/ds} d\psi. \tag{2.4}$$

Once $\psi = \psi(s)$ is known, shape of the membrane in parametric form is given by

$$x(\psi) = x(\alpha) + \int_\alpha^\psi \frac{\cos\psi}{d\psi/ds}\, d\psi, \tag{2.5}$$

$$y(\psi) = y(\alpha) + \int_\alpha^\psi \frac{\sin\psi}{d\psi/ds}\, d\psi. \tag{2.6}$$

In Appendix A we discuss arclength parameterization as well as some notes on differential geometry used here in more detail.

We study group of proteins or any other entities binding to the membrane that can be represented as solid long cylindrical objects that induce deformations on the membrane. They are characterized by a radius R and adhesion energy per unit area $(-w)$. Cylinders we consider are parallel and their length L in the z-direction is assumed to be much longer than their radius R, so we ignore any end effects.

As for the membrane, in the absence of the adhering objects it is assumed planar and is characterized by bending stiffness κ and lateral tension σ (we will discuss them in detail below). The combination $\lambda = \sqrt{\kappa/\sigma}$ defines a lenghtscale characteristic to the membrane. Membane deformations on a scale smaller than λ cost in bending energy, while deformations on a larger scale cost predominantly in tension. In the case where colloid radius is of the same order as λ bending and tension contributions become comparable and it is the balance between these two, which determines the equilibrium shape of the membrane. In fact for a typical cellular membrane tension is $\sigma \simeq 0.02 dyn/cm$ [22] and typical bending modulus is $\kappa \simeq 20 k_B T$, in which case for the characteristical length of the membrane we obtain $\lambda \simeq 64 nm$ [7]. Viral capsids are about this big, therefore biological situations are in the crossover regime.

2.2 Energy Considerations

An accurate physical description of a membrane requires knowing how its energy changes upon deformations of the membrane. First of all, it costs energy to aggregate lipids onto an interface, because the molecules have to be removed from their bulk and brought to the boundary between two phases. This energy per unit area of the membrane is called surface tension σ. The free energy of our membrane is also dependent on bending deformations of the membrane. We will consider interfaces

which can be energetically completely described by a Hamiltonian which includes surface tension and bending energies only. We discuss these two energy terms in more detail in the following sections.

2.2.1 Surface Tension

Surface tension is a result of an imbalance of the molecular forces in a media. In a liquid molecules are attracted to each other by various intermolecular forces. Those in the bulk phase, are pulled equally from all directions by neighbor molecules, which results in the net force of zero. However, at the surface of the liquid, molecules are pulled inwards by other molecules inside the liquid and since there is no attraction with the molecules from the neighboring medium, this results in the net force directed inwards at the molecules which are at the surface. This force is balanced with the liquid's resistance to compression, so net force is eventually zero. However this results in a liquid trying to squeeze together until it has the lowest surface area possible. That is why, for example, under zero gravity water forms into a perfect sphere.

Molecules at the interface have higher energy than those in the bulk, therefore one can assign a positive energy per unit area of the surface. It is usually defined as σ. It is minimal if the area of the interface is minimized, which explains the abovementioned behavior of the water in zero gravity.

The energy per unit surface area, can be interpreted also as a tension. This is best demonstrated by a rectangular piece of a surface with length l and width h at a constant temperature shown in Fig. 2.2. Now we increase the surface of the patch by applying force F on one of the sides of the patch. The free energy increase will be the applied force times the displacement and we can then write

$$dE = Fdh = F\frac{dA}{l} = \frac{F}{l}dA = \sigma dA, \tag{2.7}$$

where σ is considered as the surface tension. It is given in the units of force per unit length or energy per unit area, which are equivalent to each other. In SI units $[\sigma] = N/m$ (or in energy units J/m^2), while in cgs units it is measured in $[\sigma] = dyn/cm$ (erg/cm^2). In order to obtain the energy for the whole interface we have to integrate surface tension over the total area of the surface. Then the resulting Hamiltonian will be

$$H = \int_S \sigma \, dA, \tag{2.8}$$

where by S we denote the total area of the surface patch. For given boundary conditions, the stable surface can be found by setting variation $\delta H = 0$ and finding local minima of the Hamiltonian 2.8. This leads to the minimization of the surface area.

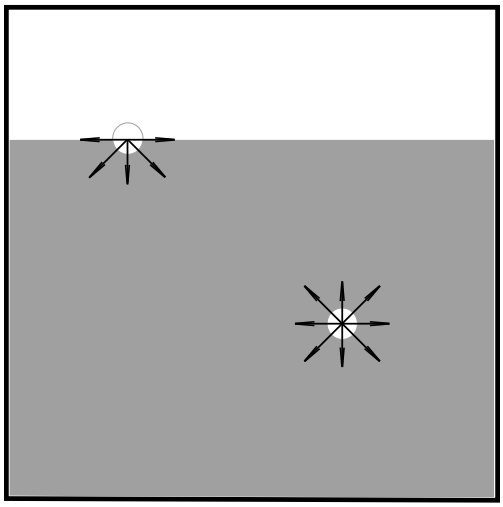

Figure 2.1: Particles on the interface are missing bonds compared to those in the bulk, therefore surface has a free energy

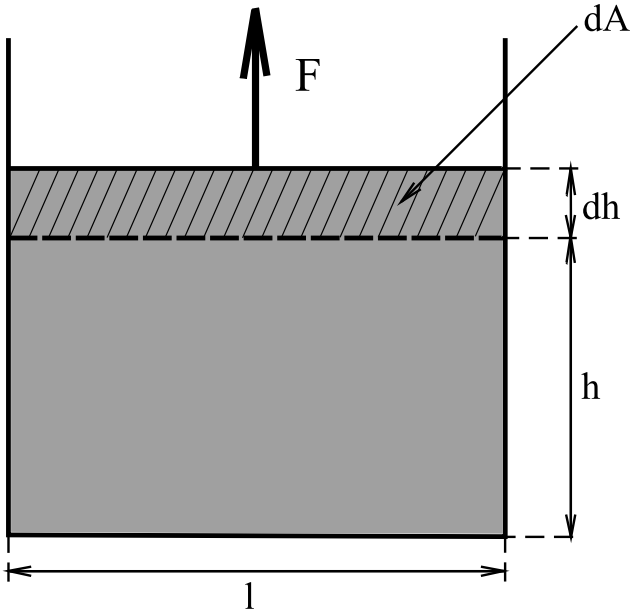

Figure 2.2: Interfacial energy interpretation as a surface tension

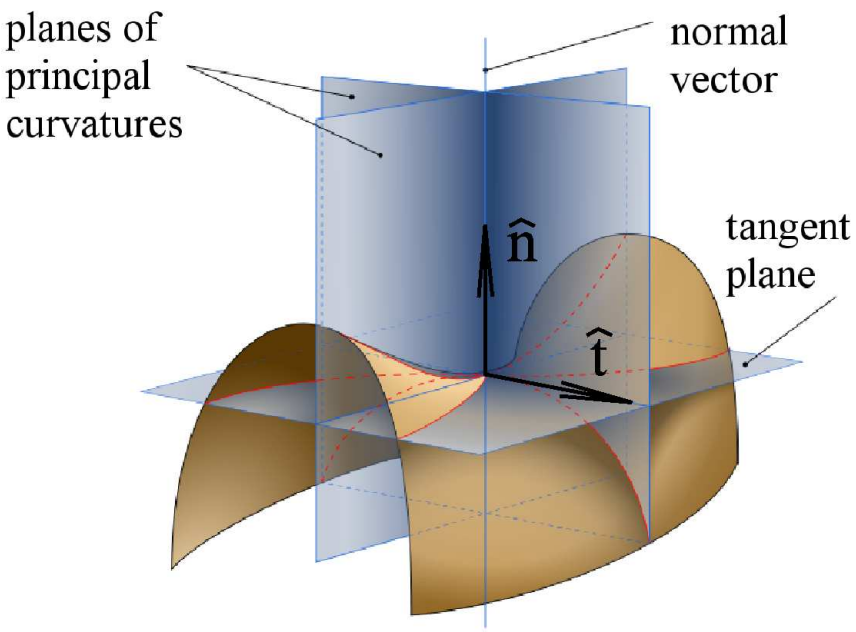

Figure 2.3: Saddle surface with the planes of principal curvatures (Author: Eric Gaba, image taken from Wikipedia)

2.2.2 Bending Energy

Next we consider the elastic energy of the membrane, which is dependent on the deformations of our membrane. We assume absence of any external fields therefore any translations and rotations of the membrane do not change its energy. But there is an elastic energy of the membrane, which is dependent on the deformations of the membrane. Generally, elastic deformation is defined as any kind of stretching of a surface. In a harmonic expansion the energy is proportional to the square of the deformation according to the Hooke's law. We consider lipid membrane, which is assumed to be an incompressible two-dimensional fluid. This means that we cannot stretch/compress them (i.e. increase or decrease the total area) by pulling it from the sides. In the context of the lipid membrane deformation is described as the bending of the membrane which still costs energy. It should be dependent on the curvature of the membrane and dependence should be quadratic.

Let's first briefly discuss what is a curvature of the membrane. Here we bring more visual explanation, for more details and definition please refer to the Appendix A. A differentiable surface at each point has a normal vector $\hat{n}$ (see Fig. 2.3). Now at that point we can construct any tangent vector to the surface. We can imagine a plane which contains the normal vector and the tangent vector $\hat{t}$. This normal flat surface will cut a plane curve from a surface which will have a curvature ζ at that point. Now, we can rotate tangent vector around normal vector $\hat{n}$, thus rotating the normal plane and changing the curve which it cuts from the surface. For different directions of the plane the curve will have different curvatures and

maximum and minimum of those at that point on the surface are called principal curvatures of the surface.

Now since at each point on the surface we have two principal curvatures we have two include two independent terms into the expression of the energy that will depend on a quadratic combination of the principal curvatures and are invariant scalars. A convenient choice is a combination of the Gaussian curvature $K_G = \zeta_1\zeta_2$ and mean curvature $K = (\zeta_1 + \zeta_2)/2$

$$H = \int_\Sigma \left[2\kappa(K - K_0)^2 + \tilde{\kappa}K_G\right] \, dA, \tag{2.9}$$

where κ and $\tilde{\kappa}$ are proportionality constants called bending rigidity and splay modulus. The constant K_0 is the spontaneous curvature and basically determines how much membrane is bend in the minimum energy state.

2.2.3 Helfrich Hamiltonian

Including the tension the complete Hamiltonian for the surface then will have the following form

$$H = \int_S \left[2\kappa(K - K_0)^2 + \tilde{\kappa}K_G + \sigma\right] \, dA. \tag{2.10}$$

This Hamiltonian was first proposed by W. Helfrich in 1973 [23] and is named after him.

The spontaneous curvature K_0 is assumed 0 further in this thesis, since we assume symmetric membrane and in equilibrium state our membrane is flat. Also no topological changes will be considered and therefore second term in 2.10 becomes 0 [1].

To sum up, it is assumed that this process can be understood as a balance of the following three energy contributions.

- Adhesion energy, which is driven by contact energy per unit area $-w$, and is proportional to contact area.
- Bending energy of the membrane, which is characterized with bending moduli of the membrane κ.
- Tension energy, which is proportional to the surface area and is characterized with lateral tension σ.

[1]The product of the two principal curvatures, ξ_1 and ξ_2 is called Gaussian curvature K_G. According to Gauss-Bonnet theorem its integral over the surface of the membrane can be rewritten as an integral over the boundary ∂S of the surface S. Therefore it is invariant under deformations of S which change neither its boundary nor topology and will result only in an constant term in energy and can be ommited [20]

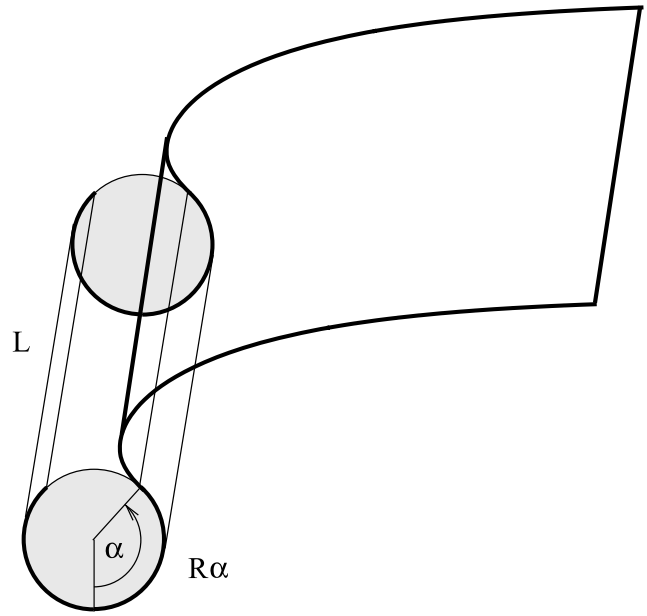

Figure 2.4: Sheet of the membrane wrapping the cylinder. The arclength of the membrane in contact with cylinder is $2R\alpha$, which multiplied by the length of the cylinder gives us the contact surface area to be $2RL\alpha$.

The total free energy of the system will be composed from the energy of the membrane which is adhered on the cylinder, and the part corresponding to the free membrane. Although finding the energy for the adhered part is relatively easy, because the shape of the membrane is already known, energy for the free part of the membrane is a functional of the shape of the membrane and needs to be minimized with respect to it first. We now discuss two cases separately.

2.2.4 Energy for the Adhered Membrane

Assuming that the adhering membrane remains in the fluid state, its energy can be calculated easily once degree of wrapping, α is known (Fig. 3.1), because the shape of the membrane is that of the cylinder it adheres to. The area of the colloid covered by the membrane is given by $A_{ad} = RL\alpha$ (see Fig. 2.4), therefore adhesion energy will be

$$E_{ad} = -w2RL\alpha. \tag{2.11}$$

For the bending part of the energy, since membrane is wrapped around the cylinder two principal curvatures are known, at any touching point one is the curvature of the circle with radius R, which is $\xi_1 = \frac{1}{R}$, while the other one is 0. (for detailed derivation please refer to the Appendix A) Bending energy will then be

$$E_{bend} = \frac{\kappa}{R^2} A_{ad} = \frac{\kappa}{R^2} RL\alpha = \frac{\kappa\alpha}{R} L. \tag{2.12}$$

Finally the work done against the lateral tension σ is proportional through σ to the excess area pulled towards the wrapping site (taking as a reference flat membrane), which is $\Delta A_{ad} = 2RL(\alpha - \sin\alpha)$, giving the tension energy

$$E_{ten} = \sigma \Delta A_{ad} = 2\sigma RL(\alpha - \sin\alpha). \tag{2.13}$$

Thus the total free energy associated with the adhered part of the membrane is a combination of the above three terms and for the contact angle α has the following form

$$E_{ad} = -2wRL\alpha + \frac{\kappa\alpha}{R}L + 2\sigma RL(\alpha - \sin\alpha). \tag{2.14}$$

We now look into the free energy of the free membrane.

2.2.5 Energy for the Free Membrane

Clearly, there is no adhesion in this case, and the only terms contributing to the free energy are the bending and tension energy terms. In this case membrane shape is not known a priori, and we need to find the membrane equilibrium profile first. The free energy F of the free membrane can be expressed as a surface integral over the bending and tension contributions and therefore is a functional of the shape. We then will minimize it with respect to the shape of the membrane and find the equilibrium state.

To write down the free energy for the problem of cylindrical colloids adhering to a fluid membrane, we use the coordinate system in Fig. 3.1, where a crossection of the cylinder and membrane is shown. The membrane shape can then be described by the tangent angle $\psi(s)$ which is a function of the contour variable s. This parameterization gives two principal curvatures of the membrane at any point as $\dot{\psi}$ and 0 (see Appendix A) and for the free part of the membrane we can write the Helfrich free energy in a simple form,

$$F = \int \left[\frac{1}{2}\kappa \left(\frac{d\psi}{ds} \right)^2 + \sigma \right] L ds, \tag{2.15}$$

where κ is the bending energy, σ surface tension and L the length of the system in the z-direction. As mentioned above, an adhering cylinder of radius R is assumed to have an adhesion energy per unit area $-w$ with the membrane. Long cylinders $L \gg R$ are assumed and we ignore any end effects.

It is convenient to introduce the following dimensionless quantities

$$\tilde{F} = FR/\kappa L \tag{2.16}$$
$$\tilde{\sigma} = \sigma R^2/\kappa \tag{2.17}$$
$$\tilde{w} = wR^2/\kappa \tag{2.18}$$
$$\tilde{s} = s/R. \tag{2.19}$$

Now with the reference to the free energy of a freely standing, planar membrane reduced free energy difference can be expressed as

$$\Delta\tilde{F} = \int \left[\frac{1}{2}\left(\frac{d\psi}{d\tilde{s}}\right)^2 + \tilde{\sigma}(1-\cos\psi) \right] d\tilde{s}. \tag{2.20}$$

This energy needs to be minimized with respect to the shape function $\psi(\tilde{s})$. Lagrange function $\Lambda = \Lambda(\dot{\psi}, \psi, \tilde{s})$ has the following form

$$\Lambda(\dot{\psi}, \psi, \tilde{s}) = \frac{1}{2}\left(\frac{d\psi}{d\tilde{s}}\right)^2 + \tilde{\sigma}(1-\cos\psi). \tag{2.21}$$

Using this in the Euler-Lagrange equation

$$\frac{\partial\Lambda}{\partial\psi} = \frac{d}{d\tilde{s}}\frac{\partial\Lambda}{\partial\dot{\psi}} \tag{2.22}$$

we obtain second-order differential equation describing the shape of the membrane $\psi(\tilde{s})$,

$$2\ddot{\psi} - \tilde{\sigma}\sin\psi = 0, \tag{2.23}$$

which has a first integral

$$\frac{1}{2}\left(\frac{d\psi}{d\tilde{s}}\right)^2 - \tilde{\sigma}(1-\cos\psi) = H, \tag{2.24}$$

where H is a constant. This first integral, together with the free energy difference above(Eq. 2.20), forms the theoretical framework for deducing the free energy of considered systems.

In the Results section we will look into three separate cases, single cylinder adhering to a membrane, two cylinders adhering at same membrane side and two cylinders adhering at different membrane sides. We will also consider the case of one and two cylinders between the solid interface and the membrane, where we consider an adhesion between the membrane and the interface.

Chapter 3

Results and Conclusions

3.1 Single Cylinder Adhered to a Membrane

We now consider the problem of a single cylinder adhering to a membrane. In an adsorbed state of single particle adhesion, the membrane wraps around the cylinder with a contact angle α (see Fig. 3.1). Membrane is asymptotically flat at $\tilde{s} \to \infty$, therefore boundary conditions $\psi \to 0$ and $\frac{d\psi}{d\tilde{s}} \to 0$ can be imposed in Eq. 2.24. This renders integration constant $H = 0$ in Eq. 2.24 and the first-integral of the Euler-Lagrange equation gets the following form

$$\frac{1}{2}\left(\frac{d\psi}{d\tilde{s}}\right)^2 - \tilde{\sigma}(1 - \cos\psi) = 0, \tag{3.1}$$

which gives us the shape equation of the membrane (right-hand side)

$$\psi(\tilde{s}) = \alpha - \sqrt{2\tilde{\sigma}} \int_0^{\tilde{s}} \sqrt{1 - \cos\psi}\, d\tilde{s}. \tag{3.2}$$

In order to obtain the parametric representation of the shape profile in Cartesian coordinate system we can use Eqs. 2.5 - 2.6 and membrane profile then can be expressed in the form

$$\tilde{x}(\psi) = \sin\alpha - \frac{1}{\sqrt{2\tilde{\sigma}}} \int_\alpha^\psi \frac{\cos\psi}{\sqrt{1 - \cos\psi}}\, d\psi, \tag{3.3}$$

$$\tilde{y}(\psi) = -\cos\alpha - \frac{1}{\sqrt{2\tilde{\sigma}}} \int_\alpha^\psi \frac{\sin\psi}{\sqrt{1 - \cos\psi}}\, d\psi. \tag{3.4}$$

For a given $\tilde{\sigma}$ increasing adhesion energy $\tilde{w}$ causes membrane to wrap cylinders more deeply with a larger contact angle α. As an example, we bring three different

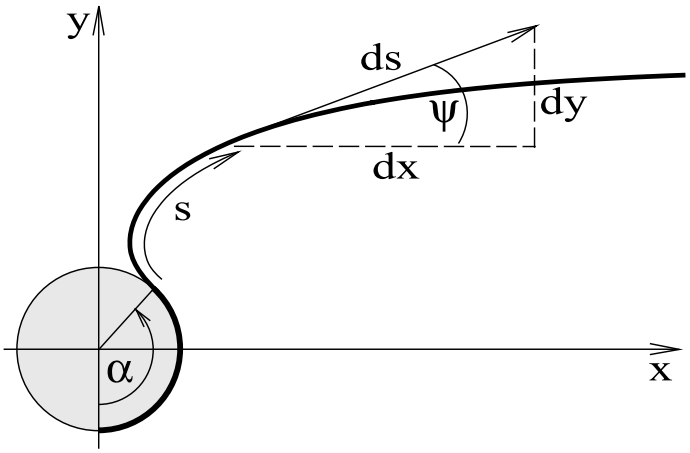

Figure 3.1: The coordinate system used to describe the shape of the membrane for single cylinder adhesion. The curve represents cross section view of membrane profile and a contact angle is denoted with α

shape profiles in Fig. 3.2 for increasing values of reduced adhesion energy $\tilde{w}$ from top to bottom. Increasing adhesion causes more wrapping and a full closure of the two sides of the membrane is expected in the large $\tilde{w}$ regime (see Fig. 3.2(C)). Contact angle at which such a closure occurs is denoted with α_{cl} and is dependent only on the characteristic parameters of the membrane. Closure point is characterized with a vanishing x-coordinate and tangential angle $\psi = \pi/2$ at the contact point, therefore closure contact angle α_{cl} can be determined requiring these conditions in the shape equation 3.3.

$$\sin\alpha_{cl} + \frac{1}{\sqrt{2\tilde{\sigma}}} \int_{\pi/2}^{\alpha_{cl}} \frac{\cos\psi}{\sqrt{1-\cos\psi}}\, d\psi = 0. \tag{3.5}$$

Carrying out the integral we have

$$\sin\alpha_{cl} + \frac{1}{\sqrt{\tilde{\sigma}}} \left[\ln\frac{\alpha/4}{\pi/8} - 2(\cos\alpha/2 - \cos\pi/4) \right] = 0. \tag{3.6}$$

From the equation above we can see that the closure angle will depend on the characteristic parameters of the membrane. On Fig. 3.3 we show the dependence of the closure angle on reduced surface tension of the membrane. Small surface tension values correspond to closure angle values close to $\pi/2$, because for angles smaller than that overhangs (and therefore closure) are generally not possible. In stronger surface tension region, where membrane is "tighter", closure angle values are higher, meaning that in the closure state, membrane wraps particles more. To

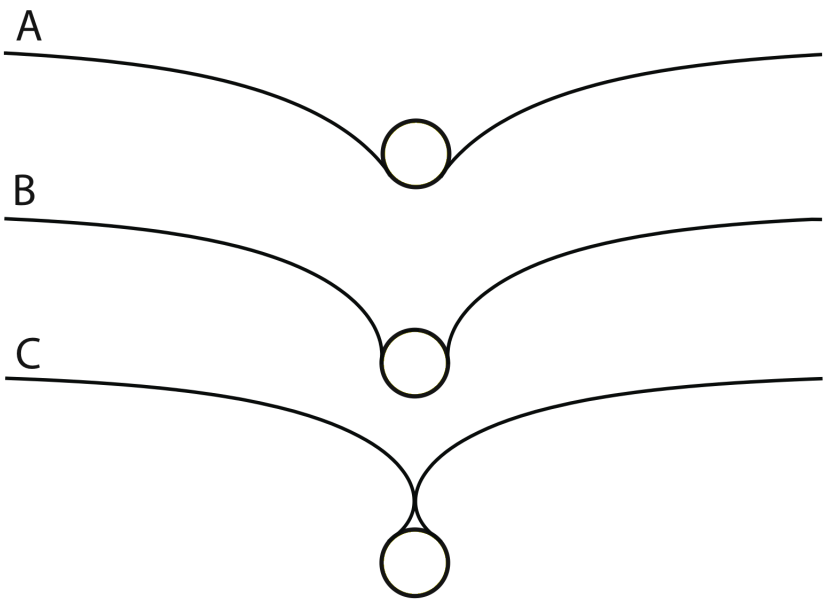

Figure 3.2: Membrane profile for (A) shallow wrapping, (B) partial wrapping and (C) closure regimes

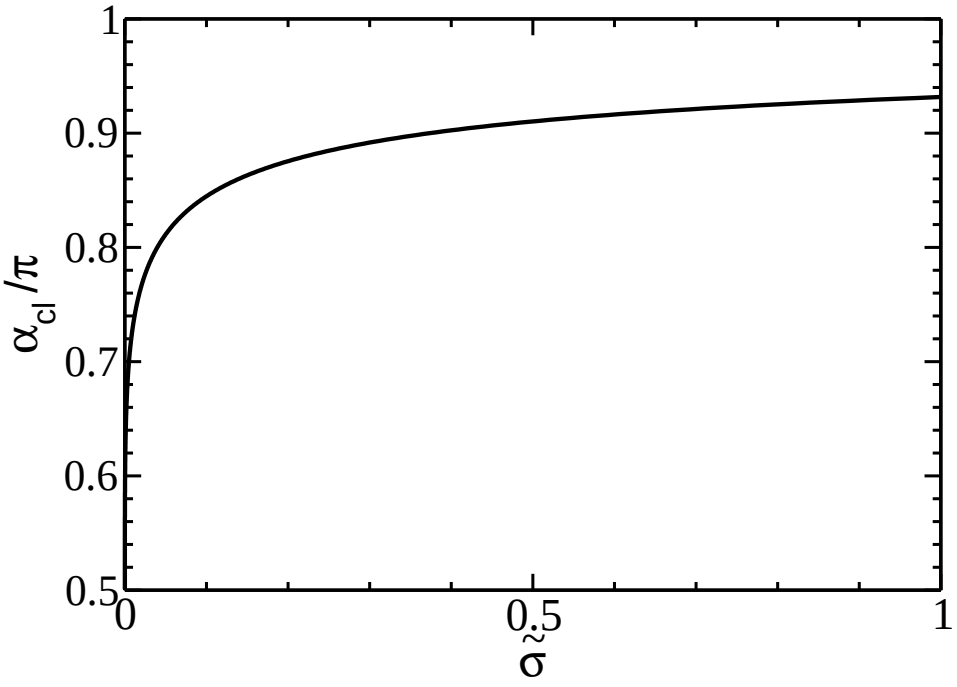

Figure 3.3: Closure angle dependence on the reduced surface tension $\tilde{\sigma}$

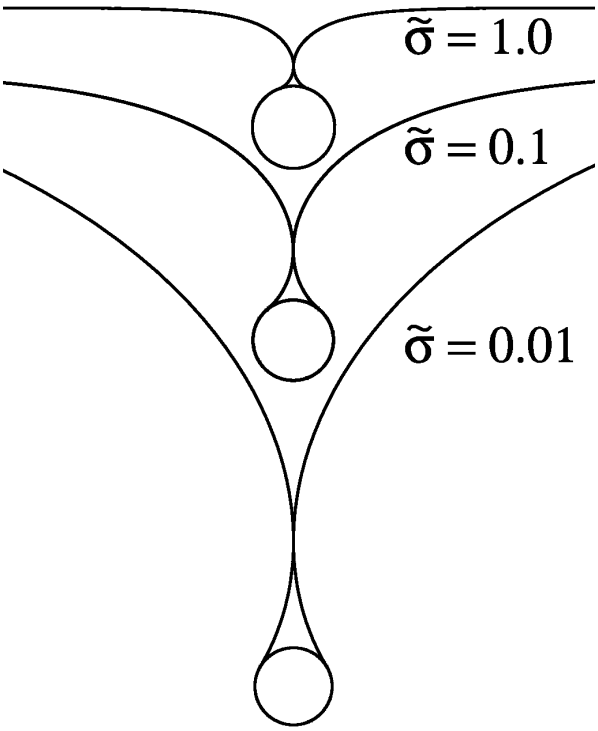

Figure 3.4: Closure state shape profiles for different reduced surface tension values

illustrate this, we plot three different closure states for different surface tension values in Fig. 3.4.

We now turn into energy considerations. Free energy of the membrane is a surface integral over bending and tension contributions and thus is a functional of its shape. For the part of the membrane adhered on the cylinder the shape of the bound part is determined by the geometry of the adhered particle, in our case it is a circular arc. Therefore, as discussed earlier, free energy of the adhered membrane part (for two sides) takes the form

$$\Delta\tilde{F}_{I(ad)} = -2\tilde{w}\alpha + \alpha + 2\tilde{\sigma}(\alpha - \sin\alpha), \tag{3.7}$$

where first term corresponds to the adhesion energy, while second and third terms are the contributions from the bending and surface tension energies correspondingly.

As mentioned above for a single cylinder case, for the free part of the membrane shape equation is found to be 3.2, using this in the Eq. 2.20, for two branches of the membrane free energy can be written as

$$\Delta\tilde{F}_I = \sqrt{8\tilde{\sigma}} \int_0^{\alpha} \sqrt{1 - \cos\psi}\, d\psi. \tag{3.8}$$

This with the energy for the adhered part of the membrane 3.7 gives us the total free energy for the membrane in the following form

$$\begin{aligned}\Delta\tilde{F}_I &= \sqrt{8\tilde{\sigma}}\int_0^{\alpha}\sqrt{1-\cos\psi}\,d\psi-(2\tilde{w}-1)\alpha+2\tilde{\sigma}(\alpha-\sin\alpha)\\ &= 8\sqrt{\tilde{\sigma}}[1-\cos(\alpha/2)]-(2\tilde{w}-1)\alpha+2\tilde{\sigma}(\alpha-\sin\alpha). \qquad (3.9)\end{aligned}$$

For different values of reduced parameters $\tilde{w}$ and $\tilde{\sigma}$, the above reduced free energy difference needs to be minimized with respect to the contact angle α.

$$\frac{\partial\Delta\tilde{F}_I}{\partial\alpha}=\sqrt{8\tilde{\sigma}}\sqrt{1-\cos\alpha}-(2\tilde{w}-1)+2\tilde{\sigma}(1-\cos\alpha)=0, \qquad (3.10)$$

$$2\tilde{\sigma}(\sqrt{(1-\cos\alpha)})^2+\sqrt{8\tilde{\sigma}}\sqrt{1-\cos\alpha}-(2\tilde{w}-1)=0, \qquad (3.11)$$

$$\sqrt{1-\cos\alpha}=\frac{-\sqrt{8\tilde{\sigma}}+\sqrt{8\tilde{\sigma}+8\tilde{\sigma}(2\tilde{w}-1)}}{4\tilde{\sigma}}. \qquad (3.12)$$

Considering the limiting values of the contact angle $\pi\geq\alpha\geq 0$, we obtain that in the regime $(\sqrt{2\tilde{\sigma}}+1/2)^2\geq\tilde{w}\geq 1/2$, where membrane is partially wrapped, a preferred cosine wrapping angle as a function of $\tilde{w}$ and $\tilde{\sigma}$ is given by the formula

$$\cos\alpha=1-(\tilde{w}^{1/2}-2^{-1/2})^2/\tilde{\sigma}. \qquad (3.13)$$

Figure 3.5 is the resulting state diagram from an analysis of the free energy 3.9. For any values of $\tilde{\sigma}$, in the region $\tilde{w}\leq 1/2$, the cylinder is in a free, adsorbed state; as $\tilde{w}$ increases crossing $1/2$, the system undergoes a second order phase transition where the membrane starts to weakly wrap the cylinder. We can expand the free energy in terms of small contact angle α.

$$\begin{aligned}\Delta\tilde{F}_I &= \sqrt{8\tilde{\sigma}}\int_0^{\alpha}\sqrt{1-\cos\psi}\,d\psi-(2\tilde{w}-1)\alpha+2\tilde{\sigma}(\alpha-\sin\alpha)\\ &= \sqrt{8\tilde{\sigma}}\int_0^{\alpha}\sqrt{1-1+\frac{\psi^2}{2}+...}\,d\psi-(2\tilde{w}-1)\alpha+2\tilde{\sigma}(\alpha-\alpha+\frac{\alpha^3}{3!}+...)\\ &= -(2\tilde{w}-1)(\alpha^{1/2})^2+\sqrt{\tilde{\sigma}}(\alpha^{1/2})^4+..., \qquad (3.14)\end{aligned}$$

where we see that $\alpha^{1/2}$ is an order parameter, in comparison with a standard Landau expansion for a second-order phase transition. This second-order phase transition was obtained earlier in [18], in a system of cylindrical colloids adhering on vesicles, where it was shown that cylindrical beads with the radius $R_0\leq(\kappa/2w)^{\frac{1}{2}}$ do not adhere on a membrane. This type of transition was obtained by Deserno et al. in [20] in a related system, where spherical colloids were discussed.

As the reduced adhesion energy $\tilde{w}$ further increases for a given $\tilde{\sigma}$, the membrane wraps the cylinder more deeply with a larger contact angle α. A full closure of the

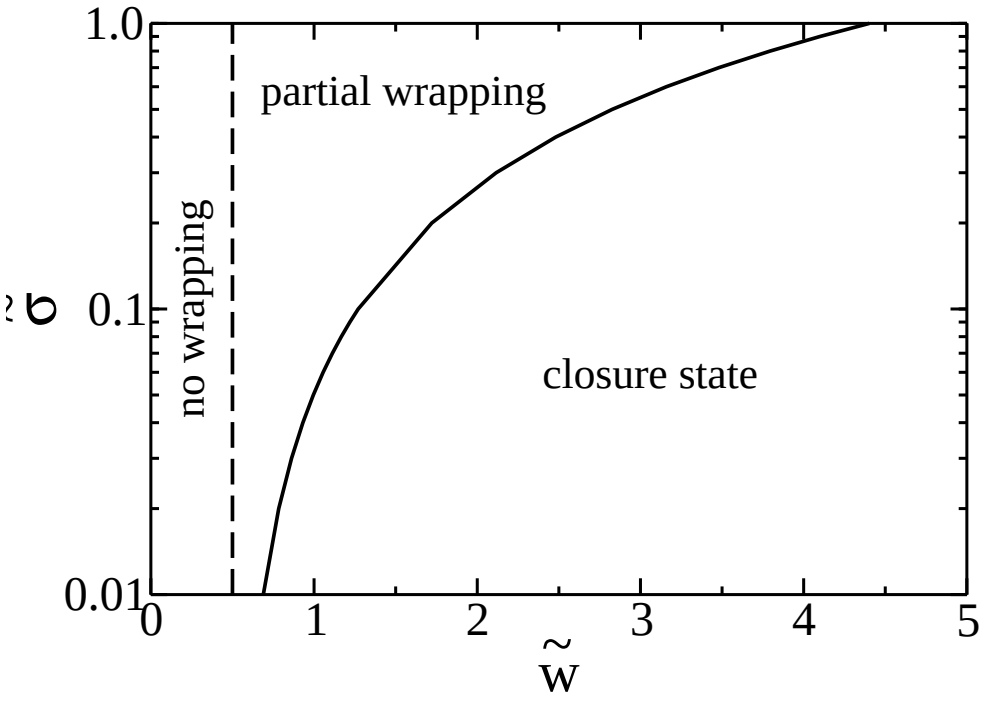

Figure 3.5: State diagram for one cylinder adhering to a membrane

two sides of the membrane is expected in the large $\tilde{w}$-regime. The closure transition can be calculated from joint consideration of Eq. 3.13 and the requirement that at the closure point of the shape curve has a vanishing x-coordinate. For a given reduced surface tension $\tilde{\sigma}$ using Eq. 3.6 we can easily obtain the value of the closure angle α_{cl}, which then can be used in Eq. 3.13 to obtain the corresponding value of $\tilde{w}$ where closure occurs. This process gives us the solid curve in Fig. 3.5.

Considering the problem of adhesion of a single spherical colloid on a membrane surface, Deserno [20] previously obtained a phase diagram qualitatively similar to ours in Fig. 3.5. The transition from no-wrapping to partial wrapping phases, for example, was also shown to be a second order transition. Furthermore, Deserno has defined a fully enveloped state where a contact angle in his system, similar to our α, attains a value of π. The transition from the partial wrapping to enveloped states was shown to be first-order by examination of the free energy. In contrast, in the cylinder adhesion case, we can show that the transition from partial to closure states is a smooth crossover with no signature of phase transition.

3.2 Two Cylinders on the Same Membrane Side

We now turn to the problem of adhesion of two parallel cylinders at the same side of a membrane. Geometry and energy aspects are already considered for the two outer sides of the membrane, so now we concentrate on the inter-cylinder membrane. Boundary conditions at the symmetry point can be imposed, where angle with

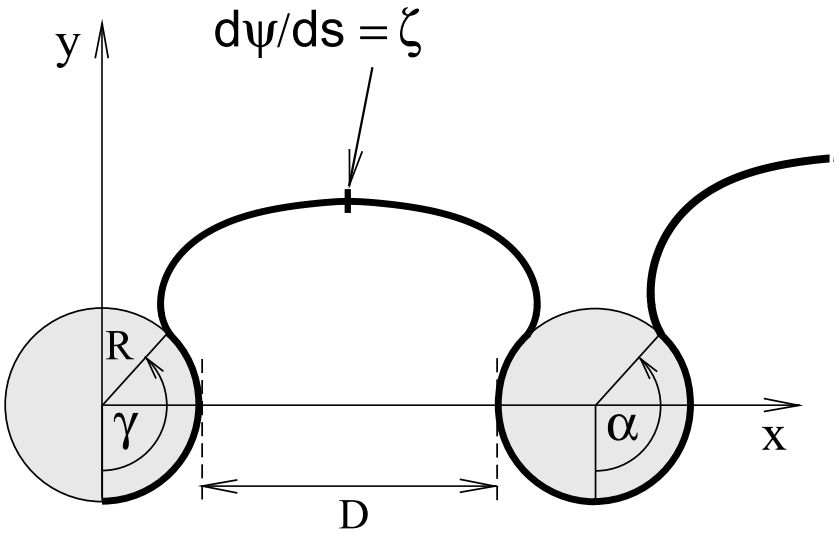

Figure 3.6: A crossection of the coordinate system used for the two-cylinder adhesion problem. The symmetric point of the membrane between the two cylinders has a curvature $d\psi/ds = \zeta$

respect to horizontal is $\psi = 0$, but now the curvature at that point is not vanishing and has a value which we denote $d\psi/ds = \zeta$ (see Fig. 3.6). Curvature in the middle decreases as we increase the distance D between the cylinders, asymptotically going to 0 when two cylinders are infinity distance apart from each other.

Imposing this boundary conditions in our Eq. 2.24 we get integration constant $H = \zeta^2/2$ and the first integral of the Euler-Lagrange equation now takes the form

$$\frac{1}{2}\left(\frac{d\psi}{d\tilde{s}}\right)^2 - \tilde{\sigma}(1-\cos\psi) = \frac{1}{2}\zeta^2. \tag{3.15}$$

From here shape equation of the profile can be found to be

$$\psi(\tilde{s}) = \gamma - \int_0^{\tilde{s}} \sqrt{\zeta^2 + 2\tilde{\sigma}(1-\cos\psi)}\, d\tilde{s}, \tag{3.16}$$

or in parametric form

$$\tilde{x}(\psi) = \sin\gamma - \int_\gamma^\psi \frac{\cos\psi}{\sqrt{\zeta^2 + 2\tilde{\sigma}(1-\cos\psi)}}\, d\psi, \tag{3.17}$$

$$\tilde{y}(\psi) = -\cos\gamma - \int_\gamma^\psi \frac{\sin\psi}{\sqrt{\zeta^2 + 2\tilde{\sigma}(1-\cos\psi)}}\, d\psi. \tag{3.18}$$

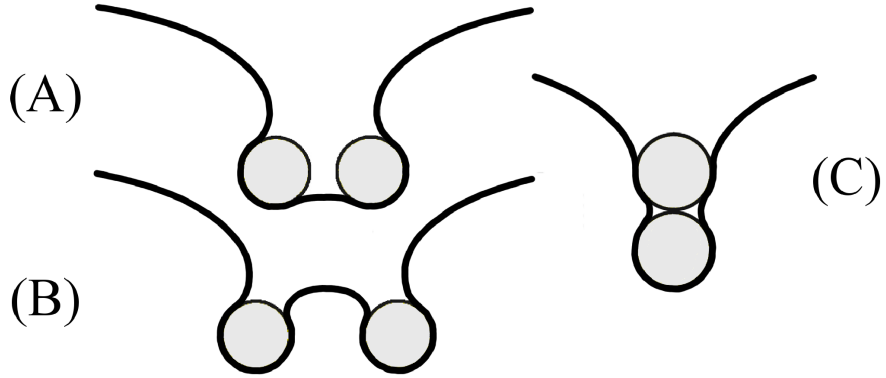

Figure 3.7: (A) Typical shallow and (B) deep wrapping shapes for two cylinders adhering to the same side of the membrane. (C) Two cylinders vertically stacked

The shape of the membrane clearly is determined by the contact angle γ and the curvature at the symmetry point ζ. Two different shape profiles are sketched on Fig. 3.7 (A) and (B). Shape (A) demonstrates typical shallow configuration of the membrane with relatively small contact angle and therefore small curvature at the symmetry point, while shape (B) corresponds to the typical deeply wrapped configuration of the membane, which is characterized by big contact angles. Clearly, for fixed distance between the cylinders, higher contact angles correspond to higher curvatures at the symmetry point.

We now look into free energy of the system. In this case free energy is separated into two parts

$$\Delta\tilde{F}_{II}(\alpha,\gamma,\zeta) = \Delta\tilde{F}_I(\alpha) + \Delta\tilde{F}'_I(\gamma,\zeta), \tag{3.19}$$

where $\Delta\tilde{F}_I(\alpha)$ describes the two branches of the membrane on the left and right sides of the system, and is identical to the free energy in Eq. 3.9. The term $\Delta\tilde{F}'_I(\gamma,\zeta)$ describes the part of the membrane between the two cylinders (see Fig. 3.6) and can also be described by the shape equation, Eq. 2.24. As mentioned above, the integration constant H in Eq. 2.24, however, is related to the curvature of membrane, $d\psi/ds = \zeta$, at the symmetric point in the middle and is found to be $H = \zeta^2/2$. Using this in Eq. 2.20, for the free energy of the membrane between the cylinders, including the contact energy, we can then write,

$$\Delta\tilde{F}'_I(\gamma,\zeta) = \int_0^\gamma \frac{\zeta^2 + 4\tilde{\sigma}(1-\cos\psi)}{\sqrt{\zeta^2 + 2\tilde{\sigma}(1-\cos\psi)}}\, d\psi - (2\tilde{w}-1)\gamma + 2\tilde{\sigma}(\gamma - \sin\gamma), \tag{3.20}$$

where γ is the contact angle shown in Fig. 3.6. For a given set of $\tilde{w}$ and $\tilde{\sigma}$ the above free energy needs to be minimized with respect to ζ and γ for a stable state.

In the following we examine the problem from a different perspective. Note that the reduced distance between the surfaces of two cylinders, $\tilde{D} \equiv D/R$, can be

γ	ζ	$\tilde{D}(\gamma,\zeta)$	$\Delta\tilde{F}'_I(\gamma,\zeta)$
0.1849	0.2250	1.0000	−0.50686
0.2227	0.2252	1.2000	−0.60917
0.2619	0.2264	1.4000	−0.71202
0.2999	0.2258	1.6000	−0.81551
0.3408	0.2272	1.8000	−0.91978
0.3802	0.2268	2.0000	−1.02494
0.4215	0.2272	2.2000	−1.13118
0.4663	0.2290	2.4000	−1.23865
0.5116	0.2302	2.6000	−1.34753
0.5560	0.2302	2.8000	−1.45820
...	...	...	...

Table 3.1: Some values from a table generated for minimizing the free energy

written by the use of the shape function and, in terms of γ and ζ, as,

$$\tilde{D}(\gamma,\zeta) = 2\int_0^{\gamma} \frac{\cos\psi}{\sqrt{\zeta^2 + 2\tilde{\sigma}(1-\cos\psi)}}\, d\psi + 2(\sin\gamma - 1). \tag{3.21}$$

In order to observe the variation of the free energy as a function of $\tilde{D}$, we have minimized the above free energy with respect to ζ and γ under this constraint. We developed a numerical procedure for this purpose, which we describe below.

Numerically the approach is to fix the distance between the cylinders, solve Eq. 3.21 to obtain the dependence of the curvature in the middle ζ on the contact angle γ (or vice versa) for this fixed distance and then, using this relation in equation for the free energy 3.20, represent it as a function of only one variable. We can then minimize it and obtain the minimum of the free energy for a given distance between the cylinders. We implement this in the way described below.

We run two nested loops (one loop inside another) for two independent parameters γ and ζ for the values they take in the intervals for contact angle $\pi \geq \gamma \geq 0$, and for the curvature $1 \geq \zeta \geq 0$. As a result we get a table, some rows of which is shown on Table 3.1, where for all the possible combinations of γ and ζ variables we have the corresponding distance between the cylinders $\tilde{D}$ and the free energy $\Delta\tilde{F}$. Note that we haven't imposed any constrains at this point, that is why the values of the obtained distances in the third column vary. The integrals for distance and free energy are calculated using standart Simpson's rule for numerical integration.

We generate this kind of tables for each fixed adhesion energy we are interested in. After having the table, it is easy to loop through it and select all the lines (i.e. pairs (γ,ζ)) which correspond to the same selected distance, and find the minimum of the free energy out of those. By doing so for different distances, we will find the minimum of the free energy as a function of distance between the cylinders.

The precision of the variables and the step size in the loops is chosen based on the region of resulting values we obtain from distance and free energy calculations. In our case, step size of 0.0002 in loops for the variables and the precision of the $4th$ digit was sufficient.

The inter-cylinder free energy is displayed as a function of $\tilde{D}$ for various values of $\tilde{\sigma}$ and $\tilde{w}$ in Figs. 3.8. Two typical membrane shapes exists between the two cylinders. In relatively small $\tilde{w}$ and large $\tilde{\sigma}$ regime, the membrane wraps two cylinders with a shallow shape, shown in Fig. 3.7(A). The solid curves in Fig. 3.8 are produced from such configurations. In the region of relatively large $\tilde{w}$ and small $\tilde{\sigma}$, a deep membrane shape can develop (Fig. 3.6(B)), which has a lower inter-membrane free energy in comparison with that of the shallow shape. The dashed curves in Fig. 3.8 are produced from deep configurations. Take the curve of $\tilde{w} = 1.1$ and $\tilde{\sigma} = 0.1$ in Fig. 3.8, for example, by increasing $\tilde{D}$, we see a first-order transition approximately at $\tilde{D} = 2.0$, signified by the crossing of the two branches of the free energy, as $\tilde{D}$ moves across the transition point, the inter-cylinder membrane abruptly jumps from shallow wrapping of the two cylinders (Fig. 3.7(A)) to deep wrapping (Fig. 3.7(B)), this transition is driven by the adhesion energy that prefers a more complete wrapping of membrane on the cylinders and is disliked by the membrane free energy that prefers a smooth variation of the shape function. In general, for systems with large $\tilde{\sigma}$, the membrane free energy dominates hence we see that the shallow shapes are more stable.

Regardless of the fact that system is in shallow or deep configurations, as $\tilde{D}$ increases the inter-cylinder free energy $\Delta\tilde{F}_I'$ generally decreases. Hence, for the problem of two cylinders adhered to a membrane surface, there is *always* a membrane-mediated repulsion interaction between the two cylinders. This conclusion has been previously drawn by Weikl [19] who has taken an approximation of the Helfrich free energy for small membrane displacement only. In such an approximation, only shallow inter-cylinder membrane can be captured. For the full wrapping this conclusion has been drawn also by Deserno using the balance of the torques for the membrane shapes. We have overlayed Weikl's estimation of the free energy in Fig. 3.8 using open squares, for every set of numerical solutions, obtained in our calculation. The comparison between our full calculation and Weikl's approximation is favorable for $\tilde{w}$ close to the free-to-partial wrapping transition, where small degree of wrapping is generally expected.

The competition between shallow and deep shapes of membrane between two colloid particles has also recently been seen in another system; when two spherical particles are confined in a cylindrical membrane tube [24], Chen et. al. showed that this competition can manifest into a more complicated phase diagram, where both attraction and repulsion between two spheres can be induced by the wrapping membrane.

We have also considered the configuration where one cylinder vertically stacks on the other one (see Fig. 3.7(C)). It was expected that for the strong adhesion energies two cylinders may prefer to stack, since in this case they will have more area

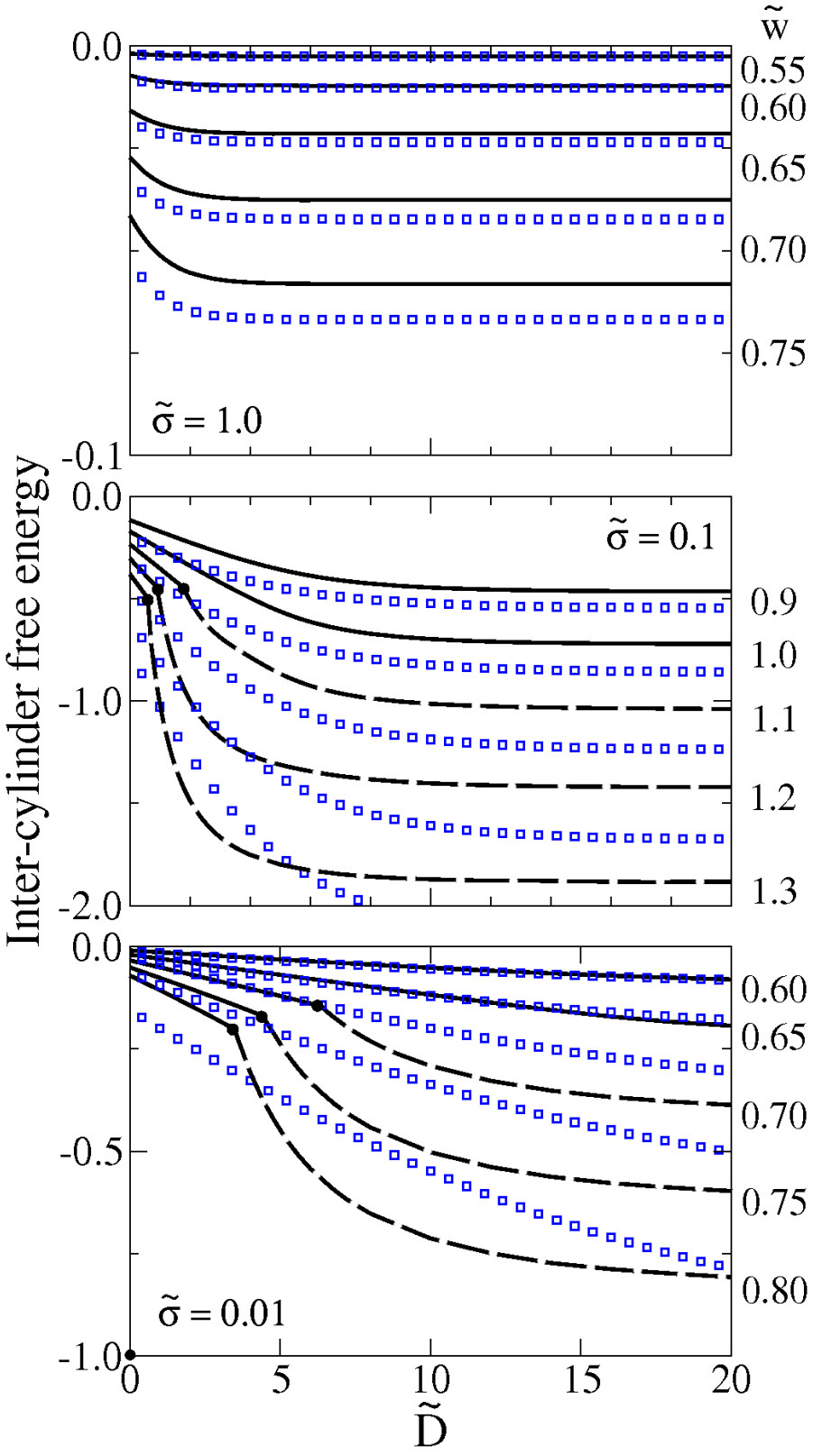

Figure 3.8: Inter-cylinder free energy dependence on surface-to-surface distance between two cylinders for three different $\tilde{\sigma}$ values

wrapped by the membrane in comparison with the case when they will be infinite distance apart. To compare the free energies for these two different configurations the following has been done.

For two cylinders at infinite distance from each other, problem is equivalent to the single cylinder case, free energy will be just doubled. As discussed, the free energy for the single cylinder for a given $\tilde{w}$ can be found by minimizing the free energy given by Eq. 3.9 with respect to contact angle α. For the same adhesion energy, we can find the free energy of the vertically stacked configuration by minimizing the free energy given by Eq. 3.20 with respect to curvature in the middle and the contact angle γ. One can plot free energy dependence on the adhesion energy for these two configurations and see if there will be a parameter region where vertically stacked phase will be preferable to the other one. We calculated the energy difference numerically in a similar way and free energy dependence on adhesion energy is shown on Fig. 3.9 for both stacked and next to each other configurations.

In the parameter regime studied here, $\tilde{w} = [1/2, 10]$ and $\tilde{\sigma} = [0.01, 1]$, we found no evidence that this types of configurations may have lower free energy than the free energy corresponding to two parallel cylinders separated far apart, each adhering to the membrane independently, which has been considered above.

In order to be able to compare with the results obtained by Deserno, in the last part of this section we want to solve the problem, where instead of constant adhesion energy, constant wrapping angle is assumed. In this case the angle $\alpha_c = \alpha_i + \alpha_o$, shown on Fig. 3.10, is assumed constant and we're interested in the equilibrium shape profiles of the membrane for different distances between the cylinders. This has been done by Deserno using the balance of the torques for different membrane shapes in [21].

We will do the following: for a given constant angle α_c, we will look into free energy dependence as a function of angle α_i. In order to compare with Deserno's results we need to plot the distance h_0 (see Fig. 3.10) of the equilibrium shape as a function of the distance between the cylinders.

We already know how to find the shape profiles for the outer and inner part of the membrane. We denote the height of the outer part of the membrane, shown on Fig. 3.10, as h_c and it can be expressed through contact angle α_o using Eq. 3.4 describing the shape profile of the membrane

$$h_c(\alpha_o) = R - R\cos\alpha_o - \sqrt{\frac{\kappa}{2\sigma}} \int_{\alpha_o}^{0} \frac{\sin\psi}{\sqrt{1-\cos\psi}}\, d\psi = R - R\cos\alpha_o + \sqrt{\frac{2\kappa}{\sigma}}\sqrt{1-\cos\alpha_o}, \tag{3.22}$$

where we will rescale this parameter with $\lambda = \sqrt{\kappa/\sigma}$ later, in order to be able to compare with the data obtained by Deserno in [21]. In the same way the height h_x

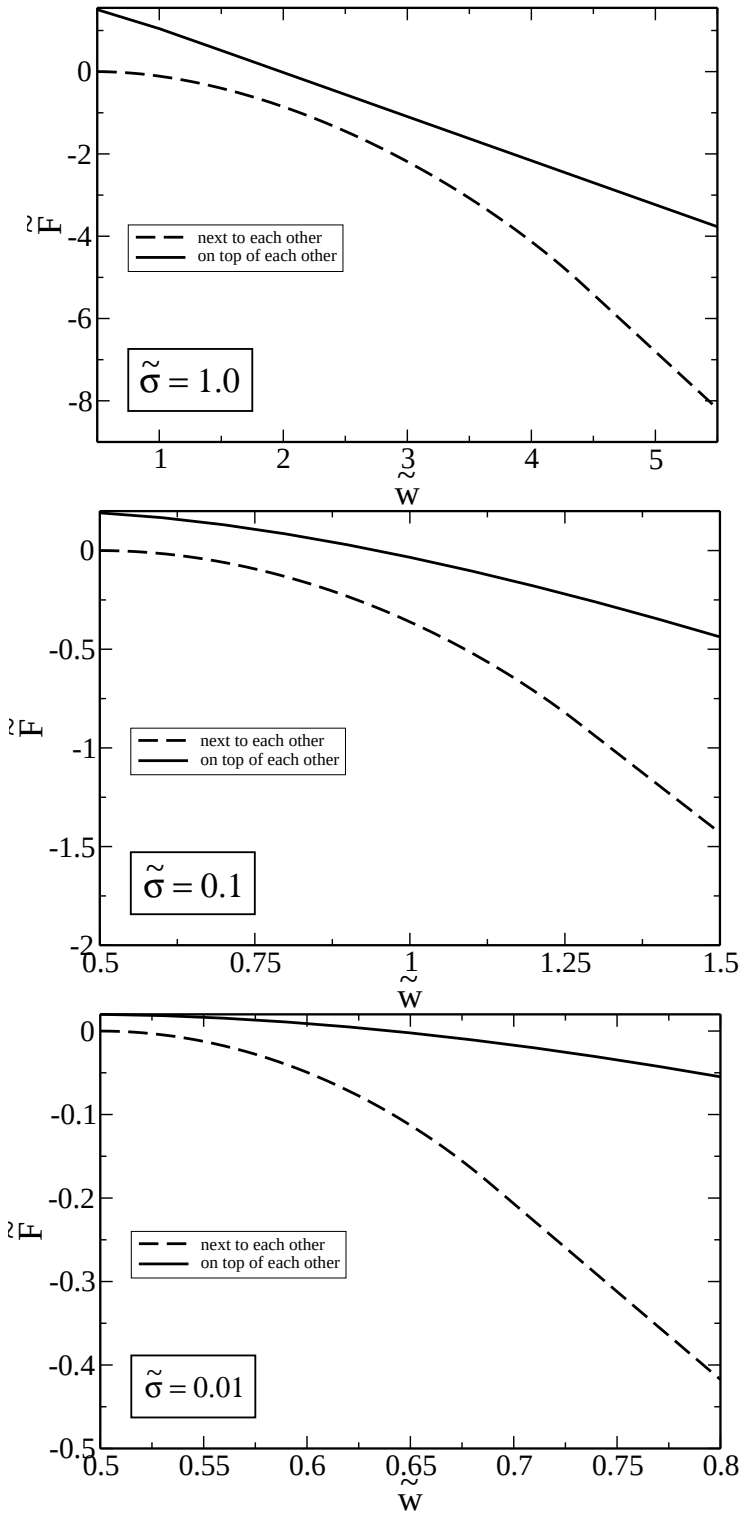

Figure 3.9: Free energy of the equilibrium shape as a function of adhesion energy $\tilde{w}$. Dashed line represents energy for configuration where two cylinders are vertically stacked, and solid line corresponds to the configuration where two cylinders are infinite distance apart

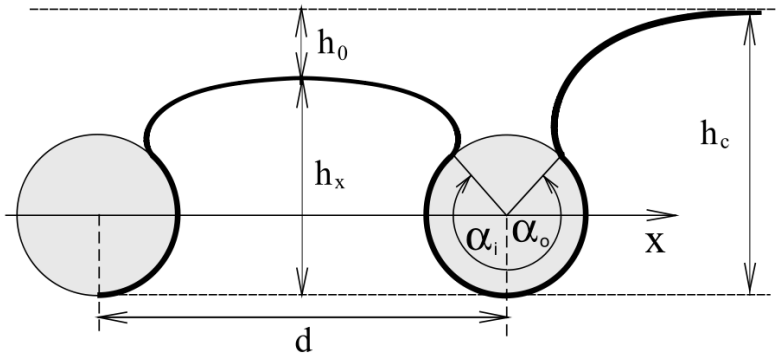

Figure 3.10: Geometry of the membrane for two cylinders adhered at same membrane side. Here $\alpha_c = \alpha_i + \alpha_o$ is assumed constant

for the inner part of the membrane can be obtained using Eq. 3.16

$$\begin{aligned} h_x(\alpha_i, \zeta) &= R - R\cos\alpha_i - \int_{\alpha_i}^{0} \frac{\sin\psi}{\sqrt{\zeta^2 + \frac{2\sigma}{\kappa}(1-\cos\psi)}}\, d\psi \\ &= R - R\cos\alpha_i + \frac{\kappa}{\sigma}\sqrt{\zeta^2 + \frac{2\sigma}{\kappa}(1-\cos\alpha_i)} - \frac{\kappa\zeta}{\sigma}. \end{aligned} \tag{3.23}$$

The distance we are interested in, h_0, can then simply be expressed as

$$h_0(\alpha_o, \alpha_i, \zeta) = h_c(\alpha_o) - h_x(\alpha_i, \zeta). \tag{3.24}$$

We are interested in the behaviour of h_0 as a function of the distance between the cylinders, which again can be expressed using shape equation 3.3

$$d(\alpha_i, \zeta) = 2(R\sin\alpha_i + \int_{0}^{\alpha_i} \frac{\cos\psi}{\sqrt{\zeta^2 + \frac{2\sigma}{\kappa}(1-\cos\psi)}}\, d\psi). \tag{3.25}$$

As we have already discussed how to obtain the free energy for this system, we can write down free energy in this case in a similar way

$$\begin{aligned} \tilde{F}(\alpha_i, \alpha_o, \zeta) = \sqrt{8\sigma\kappa}\int_{0}^{\alpha_o}\sqrt{1-\cos\psi}\, d\psi \quad &+ \quad \int_{0}^{\alpha_i} \frac{\kappa\zeta^2 + 4\sigma(1-\cos\psi)}{\sqrt{\zeta^2 + \frac{2\sigma}{\kappa}(1-\cos\psi)}}\, d\psi \\ &- \quad 4\sigma R(\sin\alpha_o + \sin\alpha_i), \end{aligned} \tag{3.26}$$

α_i	α_o	$\tilde{h}_c(\alpha_o)$	$\tilde{h}_x(\alpha_i,\zeta)$	$\tilde{h}_0(\alpha_o,\alpha_i,\zeta)$	$\tilde{d}(\alpha_i,\zeta)$	$\tilde{F}(\alpha_o,\alpha_i,\zeta)$
2.436	0.706	0.930	2.515	−1.585	2.000	−11.333
2.387	0.755	1.008	2.470	−1.462	2.100	−12.169
2.340	0.802	1.085	2.430	−1.346	2.200	−12.999
2.275	0.867	1.192	2.351	−1.159	2.300	−13.839
2.198	0.944	1.322	2.248	−0.926	2.400	−14.678
2.130	1.012	1.438	2.168	−0.730	2.500	−15.525
2.045	1.097	1.586	2.058	−0.472	2.600	−16.380
...	...	...	...	...	...	...

Table 3.2: Type of a table generated for the problem of constant wraping angle. Here distances are scaled with λ

where we omit the terms $2\frac{\kappa}{R}(\alpha_i+\alpha_o)$ (bending) and $4\sigma R(\alpha_i+\alpha_o)$ (tension), because constant wrapping angle $\alpha_i+\alpha_o$ renders those constant, and they won't play any role in minimizing the free energy.

In order to numerically obtain h_0 dependence on the distance d between the cylinders we need to find the equilibrium shape by minimizing the free energy. As above, this is done numerically. We run two nested loops through all possible values of $\alpha_0 \leq \alpha_i \leq \alpha_c$ and curvature $0 \leq \zeta \leq 1$ and generate numerical tables of the form shown in Table 3.2. For each fixed angle α_c we generate a table, which contains all possible combinations of (α_i, ζ) and the corresponding parameters in it (see Table 3.2). Note that we have only two independent parameters, α_i and ζ, since α_o is related to α_i through $\alpha_o = \alpha_c - \alpha_i$. Since we loop through α_i and ζ independently, generated table will contain different distances. We then filter those rows from the table which have the same distance and find the minimum of the free energy among those. Doing this procedure for different distances between the cylindes we obtain h_0 (or any other) parameter dependence on the distance between the cylinders.

We show on Fig. 3.11 free energy dependence on the angle α_i for several distances between the cylinders. As we can see for small distances between the cylinders, two localy stable solutions for the shape profile exist corresponding to different angles α_i. One corresponding to the smaller value of α_i is when inter-cylinder membrane is in shallow wrapping regime, and since we have fixed the total wrapping angle, outer part of the membrane has to be wrapping the cylinders deeply. The other solution corresponding to the larger value of α_i is characterized by the deeply wrapping inter-cylinder membrane and shallow wrapped outer part of the membrane (see Fig. 3.11). In this particular case, where we chose $\alpha_c = 170^o$, we see that global free energy minimum corresponds to the shape where inter cylinder membrane is in shallow wrapping regime. We will show, however, that configurations where global minimum is at the larger angle α_i are also possible.

On Fig. 3.12 we show the dependence of the height $\tilde{h}_o$ on the distance between the cylinders $\tilde{d}$ (parameters are rescaled with λ in order to compare with Deserno). Our numerical results are shown in blue color, and analytical solutions are shown

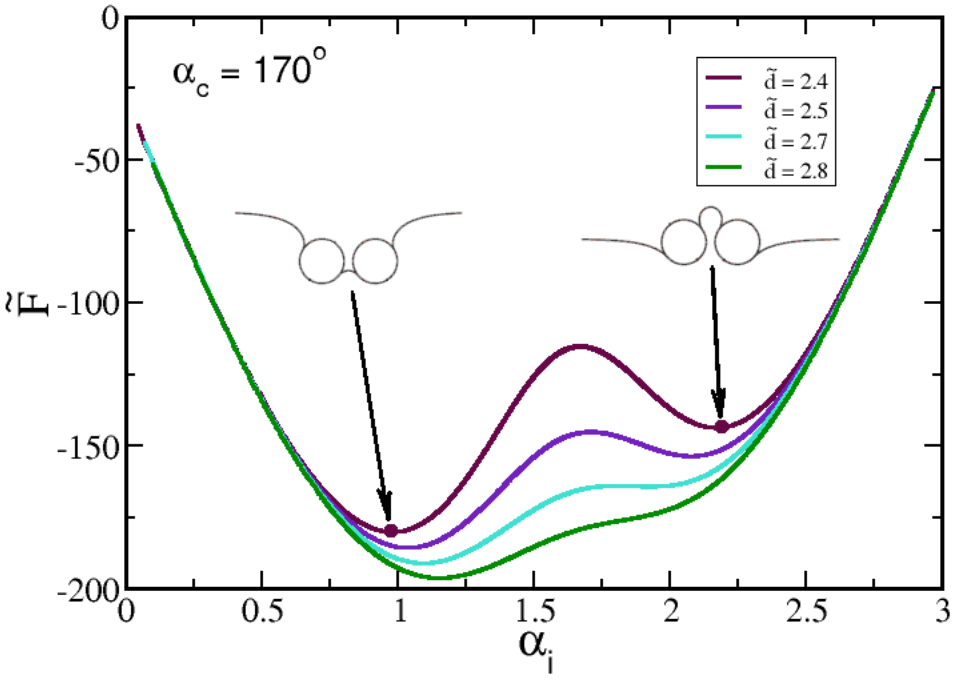

Figure 3.11: Free energy dependence on the contact angle α_i for different distances between the cylinders. Contact wrapping angle is taken $\alpha_c = 170^o$

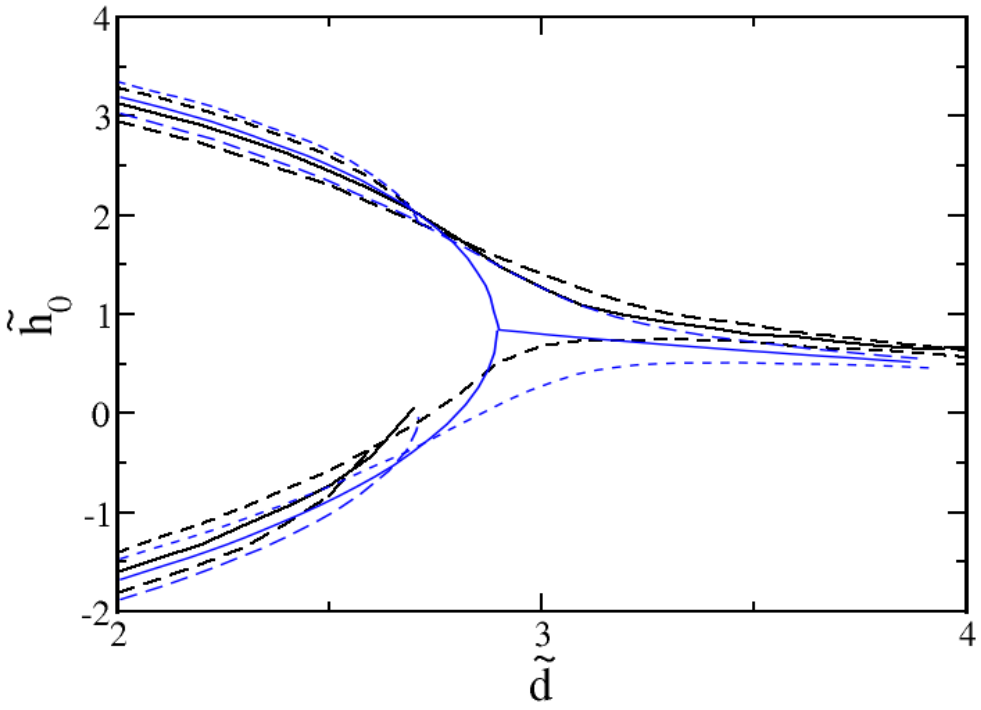

Figure 3.12: Height $\tilde{h}_0$ dependence on the distance $\tilde{d}$ between the cylinders for three different wrapping angles $\alpha_c = 170^o$ (long-dashed line), $\alpha_c = 180^o$ (solid line) and $\alpha_c = 190^o$ (short-dashed line)

in black. Three contact angles are taken, $\alpha_c = 170^o$ (long-dashed line), $\alpha_c = 180^o$ (solid line) and $\alpha_c = 190^o$ (short-dashed line). We see that for $\alpha_c = 170^o$ the global minimum is located at the smaller value of α_i, and as we increase the distance between the cylinders the minimum corresponding to the larger value of α_i vanishes. Opposite to that, for larger wrapping corresponding to the $\alpha_c = 190^o$, we see that global minimum corresponds to the larger value of the angle α_i, and the smaller-angle branch vanishes as we increase the distance.

Our result quantitatively correspond to the results previously obtained by Deserno.

3.3 Two Cylinders on the Opposite Membrane Sides

We now consider the adhesion of two cylinders on opposite sides of the membrane (see Fig. 3.13).

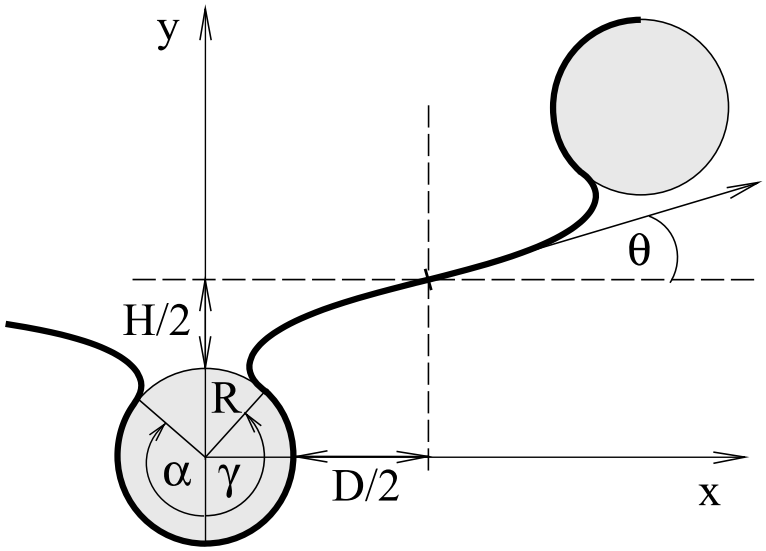

Figure 3.13: Geometry of the membrane for two cylinders adhered at opposite membrane sides. Here at symmetry point curvature is 0, and angle with respect to horizontal is denoted as θ

In this case using the coordinate system in Fig. 3.13, we see that at the middle point of the membrane stretched between two cylinders the tangent of the curve makes an angle θ with respect to the horizontal x-axis, while the curvature vanishes because of the antisymmetry. This gives us an integration constant $H = -\tilde{\sigma}(1 - \cos\theta)$ from Eq. 2.24 and we obtain first-integral of the Euler-Lagrange equation

$$\frac{1}{2}\left(\frac{d\psi}{d\tilde{s}}\right)^2 - \tilde{\sigma}(1-\cos\psi) = -\tilde{\sigma}(1-\cos\theta). \tag{3.27}$$

And therefore we can write shape equation in the following form

$$\psi(\tilde{s}) = \gamma - \sqrt{2\tilde{\sigma}} \int_0^{\tilde{s}} \sqrt{\cos\theta - \cos\psi}\, d\tilde{s}, \tag{3.28}$$

or in parametric form

$$\tilde{x}(\psi) = \sin\gamma - \frac{1}{\sqrt{2\tilde{\sigma}}} \int_\gamma^{\psi} \frac{\cos\psi}{\sqrt{\cos\theta - \cos\psi}}\, d\psi, \tag{3.29}$$

$$\tilde{y}(\psi) = -\cos\gamma - \frac{1}{\sqrt{2\tilde{\sigma}}} \int_{\gamma}^{\psi} \frac{\sin\psi}{\sqrt{\cos\theta - \cos\psi}}\, d\psi. \tag{3.30}$$

For this problem the free energy can also be separated into two parts,

$$\Delta\tilde{F}_{II}(\alpha, \gamma, \theta) = \Delta\tilde{F}_I(\alpha) + \Delta\tilde{F}'_I(\gamma, \theta), \tag{3.31}$$

where, again, $\Delta\tilde{F}_I(\alpha)$ is that considered for a single cylinder adhesion problem and $\Delta\tilde{F}'_I(\gamma, \theta)$ corresponds to the free energy between two cylinders. Taking the contact energy into account, we have

$$\Delta\tilde{F}'_I = \sqrt{2\tilde{sigma}} \int_{\theta}^{\gamma} \frac{\cos\theta - 2\cos\psi + 1}{\sqrt{\cos\theta - \cos\psi}}\, d\psi - (2\tilde{w} - 1)\gamma + 2\tilde{\sigma}(\gamma - \sin\gamma), \tag{3.32}$$

where γ is the contact angle shown in Fig. 3.13 and θ is the angle with respect to horizontal at the symmetry point.

In contrast to the three independent parameters case in the section where two cylinders were on the same side of the membrane, here the angles α, γ and θ are not independent. That is because in this case we have a constrain that the height of the membrane part on the right (or left) sides of the system should be the same as the height of the symmetry point.

We can easily find the height of the membrane from the left or right sides by solving Eq. 2.24 with a given contact angle α. In a reduced form the height of the membrane is then given by

$$\tilde{H}(\alpha) \equiv H/R = \frac{1}{\sqrt{2\tilde{\sigma}}} \int_{0}^{\alpha} \frac{\sin\psi}{\sqrt{1 - \cos\psi}}\, d\psi - 2(\cos\alpha + 1). \tag{3.33}$$

Similarly the configuration of the inter-cylinder part of the membrane can also be found using the same Eq. 2.24, but now using as boundary conditions θ and γ. The same height can be written now as

$$\tilde{H}(\gamma, \theta) = \frac{1}{\sqrt{2\tilde{\sigma}}} \int_{\theta}^{\gamma} \frac{\sin\psi}{\sqrt{\cos\theta - \cos\psi}}\, d\psi - 2(\cos\gamma + 1). \tag{3.34}$$

Equating these two equations gives rise to a constraint that governs a relationship between the three angular parameters.

$$\begin{aligned} \tilde{H}(\alpha) &= \tilde{H}(\gamma, \theta) \\ \frac{2}{\sqrt{2\tilde{\sigma}}}\sqrt{1 - \cos\alpha} - 2\cos\alpha &= \frac{2}{\sqrt{2\tilde{\sigma}}}\sqrt{\cos\theta - \cos\gamma} - 2\cos\gamma. \end{aligned} \tag{3.35}$$

Because of this constraint we can no longer treat minimization of two terms in Eq. 3.31 independently.

To study membrane-mediated interactions in this case, in the following we are interested in the free energy as a function of the reduced distance between the cylinders $\tilde{D}$, which is also a function of the γ and θ as well,

$$\tilde{D}(\gamma,\theta) = \frac{1}{\sqrt{2\tilde{\sigma}}} \int_{\theta}^{\gamma} \frac{\cos\psi}{\sqrt{\cos\theta - \cos\psi}}\, d\psi + 2(\sin\gamma - 1). \tag{3.36}$$

For this purpose, the problem is to minimise the free energy of the total system taking into account two constrains, the same $\tilde{H}$ and fixed distance $\tilde{D}$.

The numerical procedure used here is exactly the same as the one described in the section of two cylinders adhering on the same side of the membrane. The only difference is that we can choose arbitrarily two parameters, let's say α and γ , and the third parameter θ is determined from Eq. 3.35. Generation of the table and consequent search for the minimum of the free energy for fixed distance is done exactly in the same way as for the previous case.

The inter-cylinder free energy $\Delta\tilde{F}_I'$ is displayed in Fig. 3.14 for various sets of $\tilde{w}$ and $\tilde{\sigma}$. In the case of relatively weak adsorption, a typical curve contains free energy minimum somewhere below $\tilde{D} = 0$ (see, for example, the curve labeled $\tilde{w} = 1.25$ for $\tilde{\sigma} = 1.0$ case, or $\tilde{w} = 0.60$ for $\tilde{\sigma} = 0.1$ case). This usually happens for small $\tilde{w}$ where two cylinders prefer to be in shallowly wrapped configurations shown in Fig. 3.15(B) at the energy minimum. The total free energy is dominated by the contribution from the free energy cost of distorting the membrane shape on the left and right side of the system.

Previously both in small membrane deformations regime and in "geometrical" approach by Deserno distances between two cylinders less than $\tilde{D} < 0$ have not been discussed. We show that in a large $\tilde{w}$ regime, however, the system prefers to have a large contact area between cylinders and the wrapping membrane. A typical configuration of this type is shown in Fig. 3.15(C), where because of the swapping of the positions of two cylinders, the surface distance defined in Fig. 3.6 attains a value close to -4. The development of the minimum in the free energy curve near $\tilde{D} = -4$ can be viewed in the first two plots of Fig. 3.14 in a series of curves corresponding to increasing $\tilde{w}$. Note that the free energy curve has a termination point when the system is in a closure state, which is a case where two cylinders touch the membrane from the other side after the swapping of the positions. Such a closure states are indicated by filled circles on Fig. 3.14. A first order phase transition from partially wrapped state (see Fig. 3.15(B)) to a closure state (see Fig. 3.15(C)) takes place as the free energy minimum becomes deeper. We show a phase diagram based on this calculations in Fig. 3.16. In the entire parameter regime considered, the two oppositely adhered cylinders see a membrane-mediated attraction, which prefers a small separation between the two. The two attain a close contact, with a distance limited by the excluded volume between two cylinders. The conclusion of membrane-mediated attraction between two cylinders was previously suggested by Weikl, who considered a small gradient expansion of

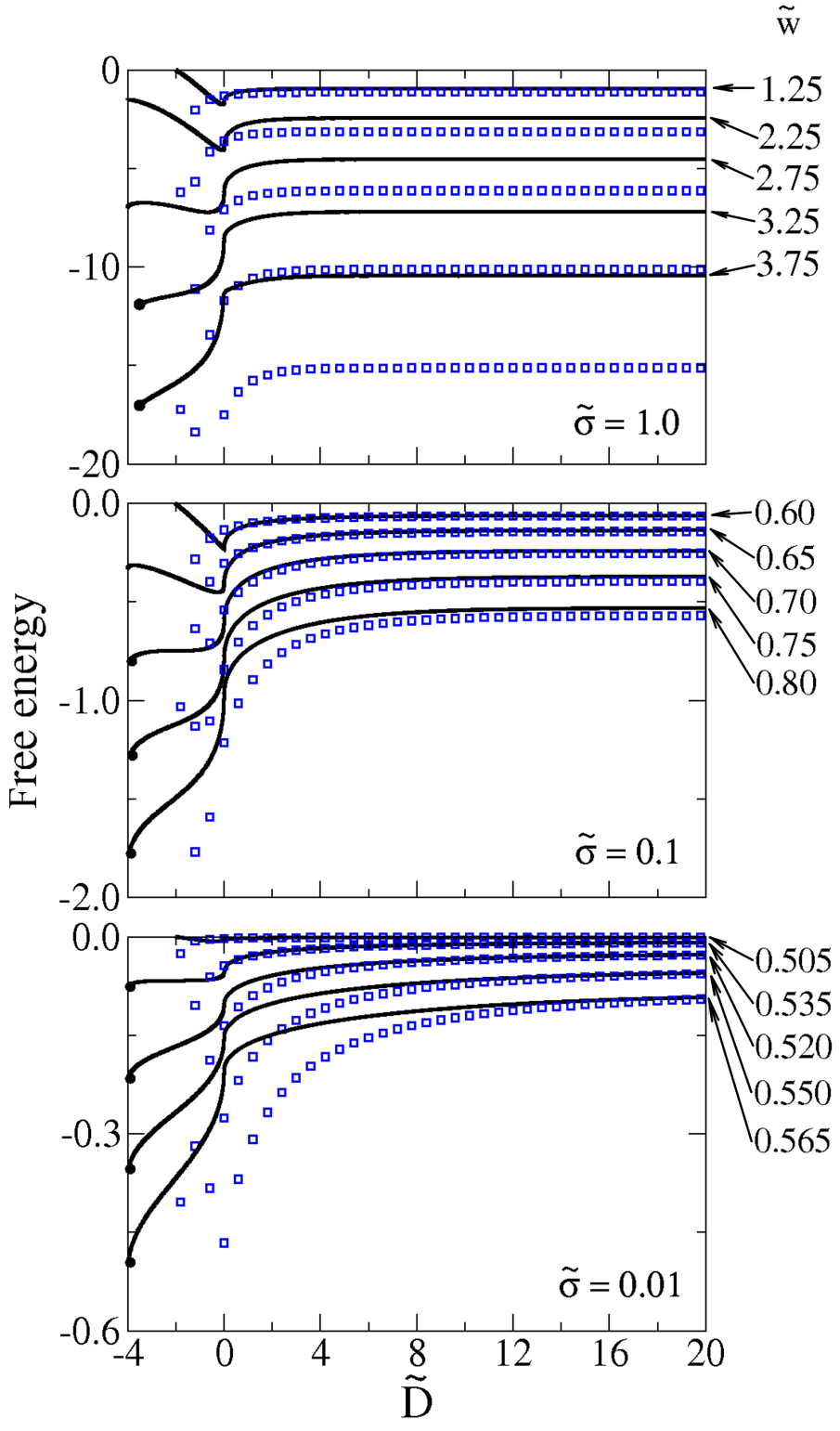

Figure 3.14: Free energy dependence on surface-to-surface distance D between the cylinders

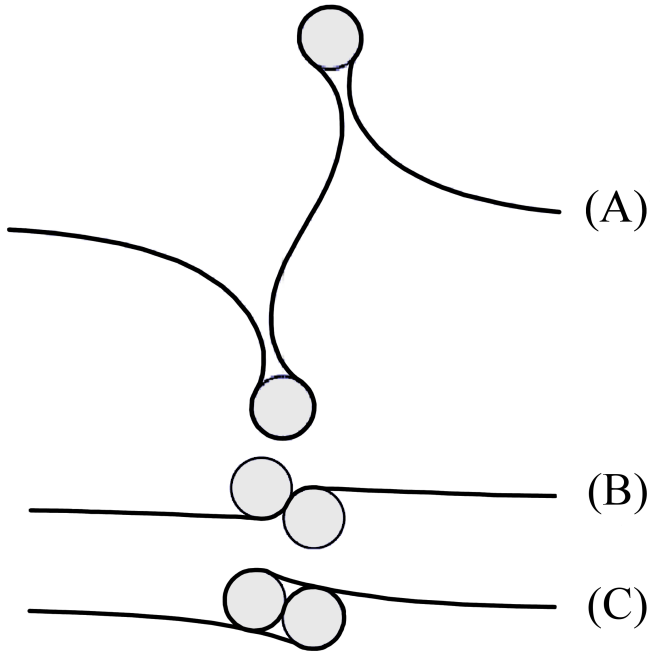

Figure 3.15: Thee example shapes of the two cylinders adhered at opposite membrane sides. (A) Example shape (B) Shallow wrapped touching state and (C) closure touching state

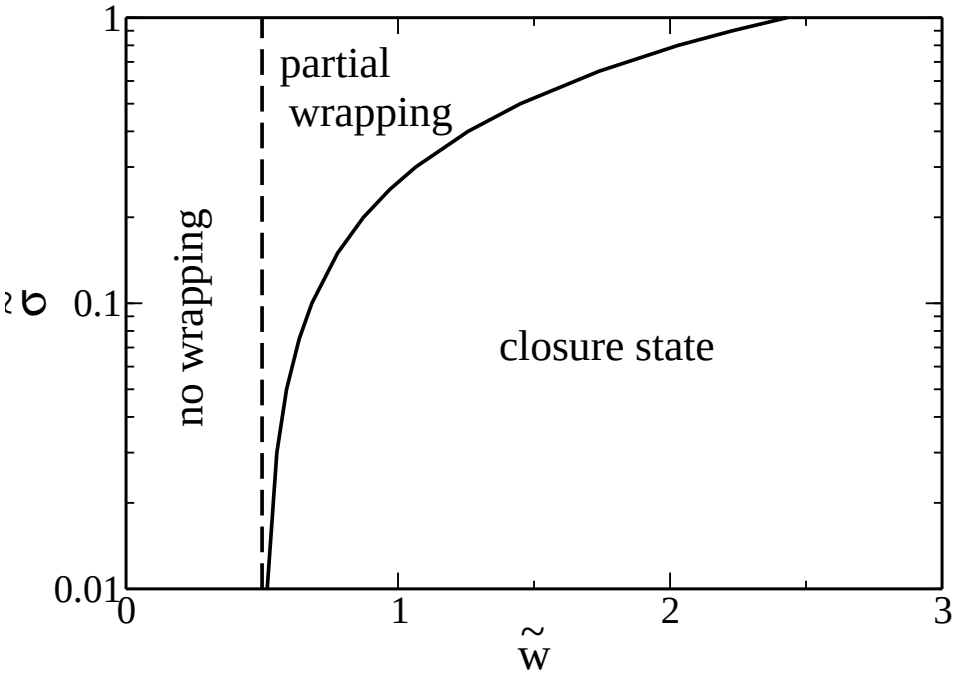

Figure 3.16: State diagram for two cylinders adhered on different membrane sides

the Helfrich model. In Fig. 3.14 we have re-plotted Weikl's approximation by open squares. Unsurprisingly, in the weak adsorption regime of the parameter space our full solution and Weikl's approximation overlap each other.

3.4 Single Cylinder Between a Membrane And an Interface

In the following sections we put a framework for the class of problems where the particle is between the membrane and the supporting interface. In this case the problem is set a bit differently in the sense that there is no adhesion between the cylinder and the membrane, but an adhesion between the membrane and the solid interface. This type of problems have experimental interest given recent research in biomedical imaging. As an example, imaging of cells involves adhering cell on an interface and consequently probing it with an atomic force microscope (see for example [25]). The framework can easily be built on the tools we have already discussed above.

We use the coordinate system shown on the Fig. 3.17. To obtain shape equation we note, that situation is very similar to the case where we had two cylinders adhering on the same side of the membrane regarding the boundary conditions, with a slight difference that here we have to make sure the symmetry point is at the interface(i.e. the height of the symmetry point is fixed). Again, we can impose, that at the contact point with the interface the angle of the tangent with respect to horizontal is equal to 0, and membrane has a curvature $d\psi/ds = \zeta$. Using this boundary conditions in the Eq. 2.24, we get the shape equations of the membrane

$$\tilde{x}(\psi) = \sin\alpha - \int_{\alpha}^{\psi} \frac{\cos\psi}{\sqrt{\zeta^2 + 2\tilde{\sigma}(1-\cos\psi)}}\, d\psi, \tag{3.37}$$

$$\tilde{y}(\psi) = -\cos\alpha - \int_{\alpha}^{\psi} \frac{\sin\psi}{\sqrt{\zeta^2 + 2\tilde{\sigma}(1-\cos\psi)}}\, d\psi. \tag{3.38}$$

Given the shape of the membrane we can find the distance D of the point along the axis x where membrane touches the interface, as well as height of the membrane H.

$$\tilde{D} = \sin\alpha + \int_{0}^{\alpha} \frac{\cos\psi}{\sqrt{\zeta^2 + 2\tilde{\sigma}(1-\cos\psi)}}\, d\psi, \tag{3.39}$$

$$\tilde{H} = 1 - \cos\alpha + \int_{0}^{\alpha} \frac{\sin\psi}{\sqrt{\zeta^2 + 2\tilde{\sigma}(1-\cos\psi)}}\, d\psi. \tag{3.40}$$

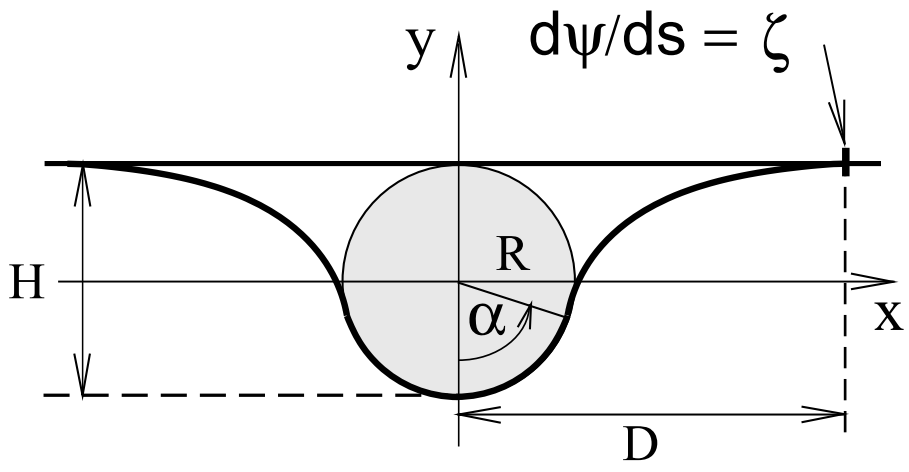

Figure 3.17: The coordinate system used to describe shape of the membrane for the single cylinder between the membrane and an interface.

We should note here that distance D determines the penalty in the free energy and is determined by the adhesion energy after finding the equilibrium shape. However height of the membrane H is not variable and should always be equal to $2R$. This is a necessary condition to make sure membrane touches the interface at some point. So we have additional condition

$$1 - \cos\alpha + \int_0^\alpha \frac{\sin\psi}{\sqrt{\zeta^2 + 2\tilde{\sigma}(1-\cos\psi)}}\, d\psi = 2, \tag{3.41}$$

which gives us the relationship between the curvature at the touching point ζ and the contact angle α. Now the integral in Eq. 3.41 can be easily solved analytically and we obtain the relationship between ζ and α in the following form.

$$\zeta^2 = \left(\frac{1-\cos\alpha}{1+\cos\alpha} - \frac{\tilde{\sigma}(1+\cos\alpha)}{2}\right)^2. \tag{3.42}$$

We show on Fig. 3.18 the curvature dependence on the contact angle α for the reduced surface tension $\tilde{\sigma} = 0.1$. We should note that the negative curvature region is forbidden, since at a contact point membrane should merge into a straight line of the interface, therefore it has to have a positive curvature. This means that for a given surface tension, there is a forbidden contact angle region, where it is impossible for the membrane to touch the interface no matter what curvature we choose. We bring different shape profiles for three different contact angles on Fig. 3.19.

We now turn to the free energy of the system. In this case we should note that there is no adhesion between the cylinder and the membrane, instead we have an

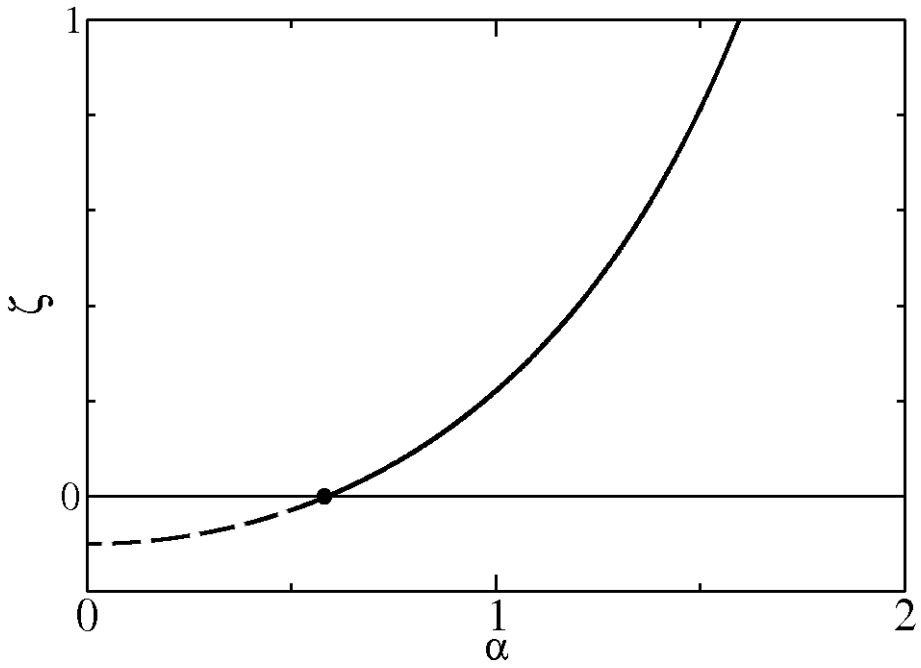

Figure 3.18: Curvature dependence on the contact angle α for the $\tilde{\sigma} = 0.1$. The dashed line indicates the forbidden region for the negative curvatures.

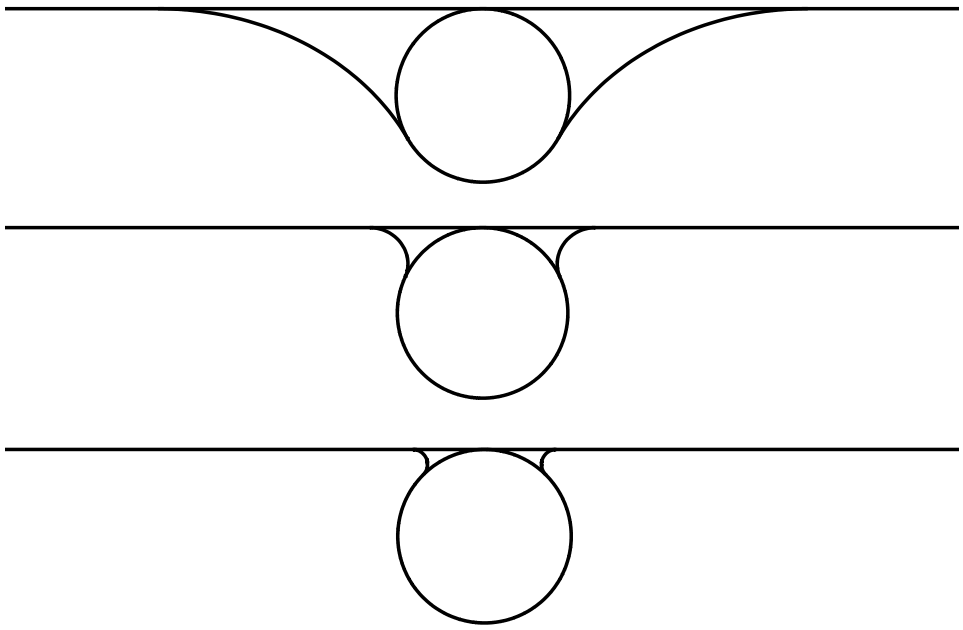

Figure 3.19: Example shape profiles for cylinder between a membrane and an interface.

adhesion between the membrane and the interface. This results in the free energy penalty which is proportional to the area of opening, since membrane prefers to have more contact with the interface. The length of the opening in in x-direction is shown on the Fig. 3.17 as D. The rest of the energy functional is exactly the same as in two cylinders case, except that care needs to be taken for the adhesion part. We write energy functional in the following form.

$$\Delta\tilde{F}_I = \int_0^\alpha \frac{\zeta^2 + 4\tilde{\sigma}(1-\cos\psi)}{\sqrt{\zeta^2 + 2\tilde{\sigma}(1-\cos\psi)}}\, d\psi + \alpha + 2\tilde{\sigma}(\alpha - \sin\alpha) + 2\tilde{w}\tilde{D}, \tag{3.43}$$

where after using the expression for distance D from Eq. 3.39 we obtain

$$\Delta\tilde{F}_I = \int_0^\alpha \frac{\zeta^2 + 4\tilde{\sigma}(1-\cos\psi)}{\sqrt{\zeta^2 + 2\tilde{\sigma}(1-\cos\psi)}}\, d\psi + \alpha + 2\tilde{\sigma}(\alpha - \sin\alpha) \tag{3.44}$$

$$+ \quad 2\tilde{w}(\sin\alpha + \int_0^\alpha \frac{\cos\psi}{\sqrt{\zeta^2 + 2\tilde{\sigma}(1-\cos\psi)}}\, d\psi). \tag{3.45}$$

Now the relation between ζ and α makes energy functional dependent only on the contact angle α. This means that for given w to find the equilibrium shape we need to minimize the free energy functional only with respect to the contact angle α.

We plot the free energy as a function of the contact angle α for the different values of $\tilde{w}$ on Fig. 3.20. We see that for the fixed adhesion energy there is an optimal shape corresponding to the minimum of the free energy. Higher adhesion energies correspond to more wrapped states.

3.5 Two Cylinders Between a Membrane and an Interface

We now turn into the problem of the two cylinders between the membrane and a solid interface. The schematic illustration of the system in shown on Fig. 3.21, where now with D we denote the center-to-center distance between the cylinders and with D_x the length of the opening of the each cylinder (on one side).

Here when writing free energy we need to take into account the distance between the cylinders. In the general case, when the distance between the cylinder is much larger than two openings for the inner side of the membrane $D \gg 2D_x$ free energy can be written using previously obtained result for the single cylinder 3.45. It has

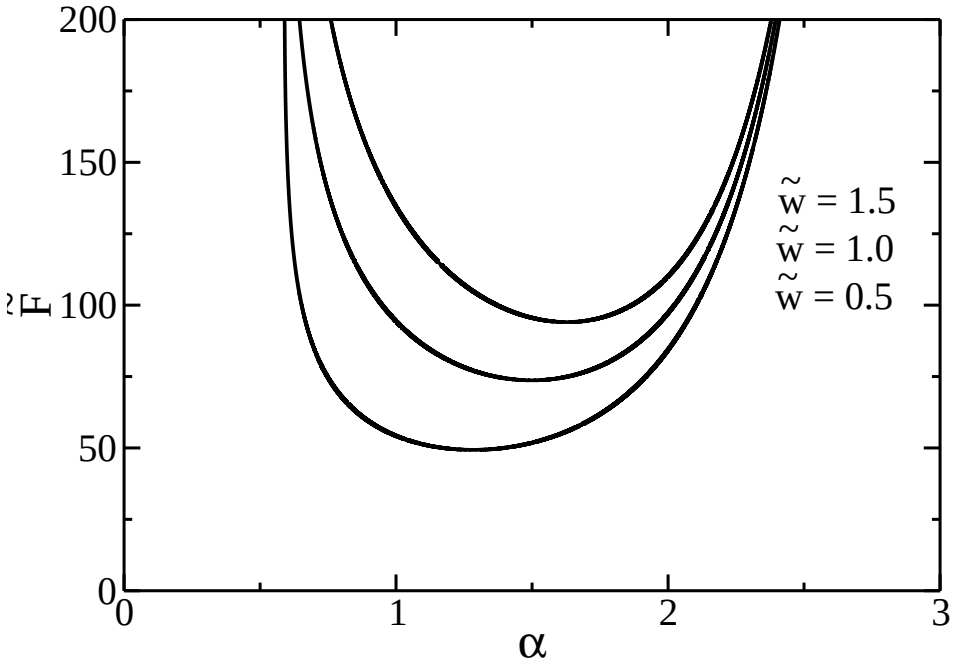

Figure 3.20: Free energy dependence on the contact angle for three different adhesion energies.

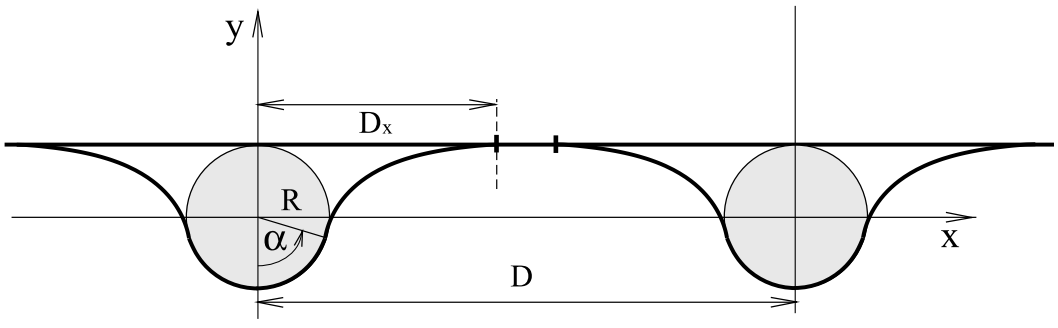

Figure 3.21: Schematic diagram for two cylinders between the membrane and a solid interface. Distance D denotes the center-to-center distance between the cylinders, and distance D_x denotes the length of the opening for each cylinder

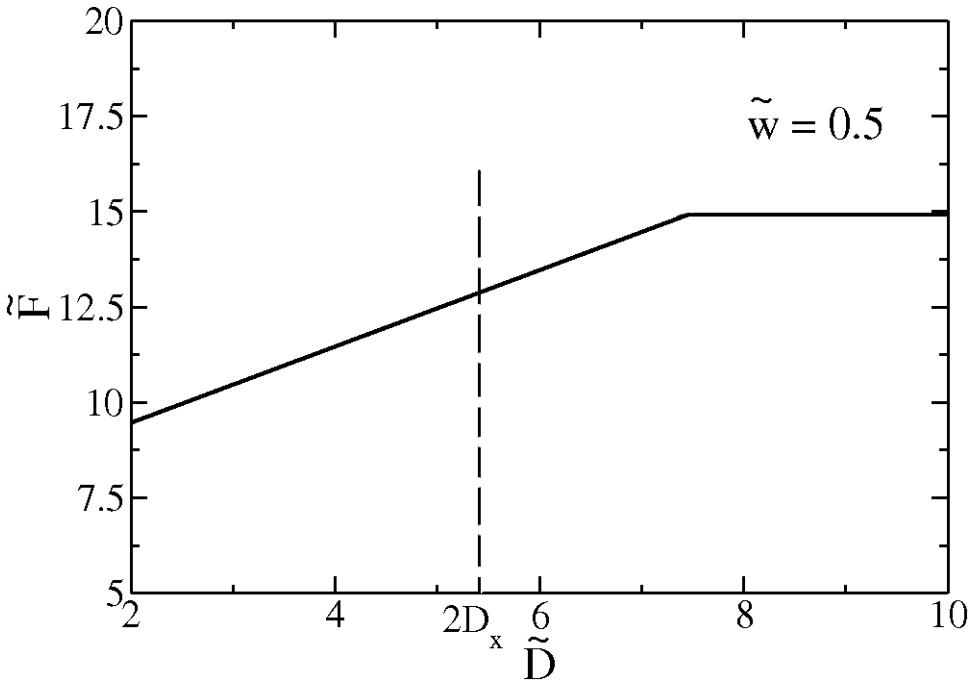

Figure 3.22: Free Energy of the system with two cylinders between a membrane and an interface as a function of the distance between the cylinders

the following form

$$\Delta\tilde{F}_I = 2\int_0^{\alpha} \frac{\zeta^2 + 4\tilde{\sigma}(1-\cos\psi)}{\sqrt{\zeta^2 + 2\tilde{\sigma}(1-\cos\psi)}}\, d\psi + 2\alpha + \tilde{\sigma}(\alpha - \sin\alpha) \tag{3.46}$$

$$+ \quad 4\tilde{w}(\sin\alpha + \int_0^{\alpha} \frac{\cos\psi}{\sqrt{\zeta^2 + 2\tilde{\sigma}(1-\cos\psi)}}\, d\psi). \tag{3.47}$$

Now if we move cylinders further apart free energy won't change, since the penalty opening area will remain the same. The situation changes however if we start bringing cylinders together. We show free energy dependence on the distance between the cylinders on the Fig. 3.22. Note that at some point, where cylinders are close enough, it is no longer advantageous for the intercylinder membrane to touch the surface, because the adhesion energy it gains from that contact is not sufficient to compensate the bending of the membrane. Inter-membrane shape jumps from wrapped to not wrapped state (see Fig 3.23), with a characteristically first-order transition. Note however, that transition point comes earlier than the point where two cylinders are separated with a distance $2D_x$, which is shown on Fig. 3.22 with a dashed line. It is easily explained, given the fact that the adhered part of the membrane compensates bending.

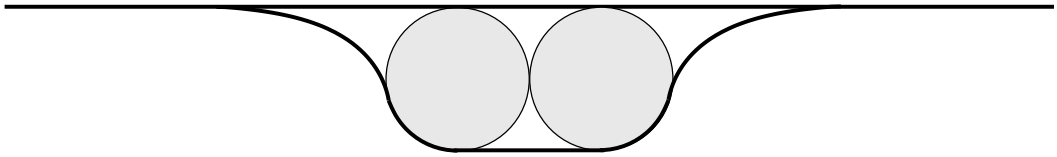

Figure 3.23: Membrane profile for the shallow wrapping case when two cylinders are separated with the distance $D <= 2D_t$

3.6 Conclusions

We have looked into adhesion and membrane-induced interaction of cylindrical colloids on a fluid membrane. For a colloid adhesion on a membrane we discussed separately three different cases: one cylinder adhering on a membrane, two cylinders adhering on the same side of the membrane and two cylinders adhering at opposite sides of the membrane. For a single cylinder we separate on a diagram three states, no wrapping, partial wrapping and closure states. The results are then compared to the analogious state diagram for a spherical colloids obtained in other work.

For the two cylinders adhering on the same side of the membrane we obtain always repulsive interaction and a transition from shallow to deep wrapping as cylinders move further apart. Based on full treatment of the Helfrich model, we have shown that deep wrapping of the membrane on cylinders can cause significant structure behaviour that is much richer than the theoretical results obtained from a small gradient expansion approximation. For two cylinders on the same side case, we have obtained a new free energy branch that was not considered before, which is characterisez by the fact that system jumps into deep wrapping regime.

For two cylinders case adhering at opposite sides of the membrane, we have shown that interaction is always attractive and two cylinders are generally in contact. We have considered further after the contact and showed that a first order transition from shallow to full wrapping is possible.

In the last section we put a framework for another class of problems, where this model can easliy be applied. In these kind of problems colloidal objects are between the membrane adhering on an interface. This kind of systems are often encountered in the medical imaging techniques.

APPENDICES

Appendix A

Some Notes on the Differential Geometry of Two-Dimensional Surfaces

A.1 Surface Definition

Let U be an open subset of $\mathbb{R}^2$. We can define a function

$$\vec{r}: \begin{cases} \mathbb{R}^2 \supset U & \to \mathbb{R}^3 \\ (u^1, u^2) & \mapsto \vec{r}(u^1, u^2). \end{cases} \tag{A.1}$$

Such a mapping defines a smooth surface patch S embedded in three dimensional Euclidian space $\mathbb{R}^3$. We can then define two vectors

$$\mathbf{e}_\mu \equiv \vec{r}_{,\mu} := \frac{\partial \vec{r}}{\partial u^\mu}, \tag{A.2}$$

which are two linearly independent tangential vectors to the surface patch S at the point $\vec{r}(u^1, u^2)$. Any other tangential vector at that point can be represented as a linear combination of $\mathbf{e}_1$ and $\mathbf{e}_2$. We can also define a normal vector to the surface at the same point $\vec{r}(u^1, u^2)$ as

$$\vec{n} := \frac{\mathbf{e}_1 \times \mathbf{e}_2}{|\mathbf{e}_1 \times \mathbf{e}_2|}. \tag{A.3}$$

Note that by definition $\vec{n}$ is a unit vector while $\mathbf{e}_\mu$ are generally not. Together they form a local basis in $\mathbb{R}^3$

$$\mathbf{e}_\mu \cdot \vec{n} = 0 \text{ and } \vec{n} \cdot \vec{n} = 1. \tag{A.4}$$

A.2 The Metric Tensor

Once we know the tangent vectors, we can define the metric tensor, or first fundamental form of the surface as

$$g_{ij} := \mathbf{e}_i \cdot \mathbf{e}_j \tag{A.5}$$

This is a second-rank, diagonal tensor. Its dual tensor is denoted as g^{ij} and is such that the following is satisfied

$$g_{ij} g^{jk} = \delta_i^k, \tag{A.6}$$

where δ_i^k is the Kronecker symbol. Therefore the components of the inverse metric are given by

$$\begin{pmatrix} g^{11} & g^{12} \\ g^{21} & g^{22} \end{pmatrix} = \frac{1}{g} \begin{pmatrix} g_{22} & -g_{21} \\ -g_{12} & g_{11} \end{pmatrix}, \tag{A.7}$$

where by g we denote the determinant of the metric tensor

$$g := \det \mathbf{g} = \frac{1}{2} \varepsilon^{ik} \varepsilon^{jl} g_{ij} g_{kl}. \tag{A.8}$$

In the above expression we used two-dimensional Levi-Civita symbol ε^{ik}, which is defined as

$$\varepsilon^{ik} = \delta_1^i \delta_2^k - \delta_1^k \delta_2^i. \tag{A.9}$$

The infinitesimal distance between two points on the surface can be written through the metric in the following way

$$\begin{aligned} ds^2 &= [\vec{r}(u^1 + du^1, u^2 + du^2) - \vec{r}(u^1, u^2)]^2 = \left(\frac{\partial \vec{r}}{\partial u^1} du^1 + \frac{\partial \vec{r}}{\partial u^1} du^2 \right)^2 \\ &= (\mathbf{e}_1 du^1 + \mathbf{e}_2 du^2)^2 = (\mathbf{e}_i du^i)^2 = (\mathbf{e}_i \cdot \mathbf{e}_j) du^i du^j = g_{ij} du^i du^j. \end{aligned} \tag{A.10}$$

A.3 The Extrinsic Curvature Tensor

Now let's assume there is a curve C defined on a surface patch S. The curve is parameterized as $\vec{r}(u^1(s), u^2(s))$, where s is the arclength of the curve. At any point P on the curve C we can construct a tangent vector $\vec{t} = \dot{\vec{r}}$ and a principal normal vector $\vec{p} = \dot{\vec{t}}/|\dot{\vec{t}}| = \dot{\vec{t}}/\zeta$, where dot indicates derivative with respect to arclenght s. If the angle between $\vec{p}$ and $\vec{n}$ is denoted by θ (see Fig. A.1) we can then write

$$\vec{p} \cdot \vec{n} = \cos\theta \text{ and } \dot{\vec{t}} = \zeta \cdot \vec{p} \tag{A.11}$$

We can combine these two and write

$$\zeta \cos\theta = \dot{\vec{t}} \cdot \vec{n} \tag{A.12}$$

Since the curve is given in a parametric form as $u^i(s)$ we can then write

$$\dot{\vec{t}}(s) = \ddot{\vec{r}}(s) = \frac{\partial^2 \vec{r}(s)}{\partial s^2} = \frac{\partial}{\partial s} \left(\frac{\partial \vec{r}}{\partial u^i} \dot{u}^i \right) = \frac{\partial^2 \vec{r}}{\partial u^i \partial u^j} \dot{u}^i \dot{u}^j + \frac{\partial \vec{r}}{\partial u^i} \ddot{u}^i \tag{A.13}$$

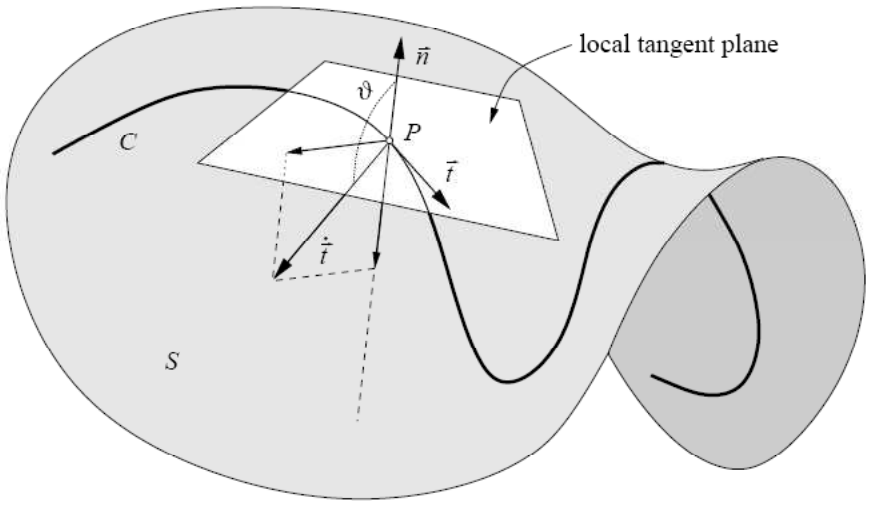

Figure A.1: Illustration of the normal curvature ζ_n (image is taken from reference [26])

and using the definition of tangential vectors A.2 we can write this in the following form

$$\dot{\vec{t}}(s) = \mathbf{e}_{i,j}\dot{u}^i\dot{u}^j + \mathbf{e}_i\ddot{u}^i \tag{A.14}$$

Using this in Eq. A.12 and the fact that $\mathbf{e}_i \cdot \vec{n} = 0$ we obtain

$$\zeta\cos\theta = \dot{\vec{t}}\cdot\vec{n} = (\mathbf{e}_{i,j}\cdot\vec{n})\dot{u}^i\dot{u}^j \tag{A.15}$$

Left hand side of the expression is called the normal curvature of the surface. It is defined as

$$\zeta_n = \zeta\cos\theta = (\mathbf{e}_{i,j}\cdot\vec{n})\dot{u}^i\dot{u}^j. \tag{A.16}$$

The expression in the brackets is not dependent on the curve, but is a property of the surface and is called the extrinsic curvature tensor or the second fundamental form. It is usually denoted with b_{ij} and is given by the formula

$$b_{ij} = \mathbf{e}_{i,j}\cdot\vec{n}. \tag{A.17}$$

We can do reparameterization of the curve, and using

$$\dot{u}^i = (du^i/dt)(dt/ds) = u^{i'}/s' \tag{A.18}$$

And using this in A.15 we obtain

$$\zeta_n = \zeta\cos\theta = b_{ij}\dot{u}^i\dot{u}^j = \frac{b_{ij}u'^iu'^j}{s'^2} = \frac{b_{ij}u'^iu'^j}{g_{ij}u'^iu'^j}, \tag{A.19}$$

where on the last step we used A.11. This shows that the normal curvature can be represented as a ratio between the second and first fundamental forms.

More visually, it can be understood in the following way. At a point P normal vector $\vec{n}$ (to the surface) and tangential vector $\vec{t}$ can be constructed. Now we can imagine a plane going through these two vectors which will cut a flat curve from the surface. The curvature of that flat curve at a point P (which is simply determined from the radius of osculating circle at that point) is exactly the normal curvature of the surface on that point in the direction of tangent vector. Now we can rotate the tangent vector at the same point P, which will rotate the plane and therefore the flat curve which the plane cuts from the surface will change. Then a natural question comes, in which directions normal curvature is extremal. To understand that we can re-write the Eq. A.19 in a little bit different form.

$$(b_{ij} - \zeta_n g_{ij})v^i v^j = 0 \tag{A.20}$$

And after differentiating with respect to v^k we obtain

$$(b_{ik} - \zeta_n g_{ik})v^i = 0 \tag{A.21}$$

and to raise the index, we multiply with metric g^{kj} and obtain

$$(b_i^j - \zeta_n \delta_i^j)v^i = 0 \tag{A.22}$$

This shows that to find the extremal normal curvatures at point P we have to solve an eigenvalue problem. Eigenvectors of matrix b_i^j will give us the directions along which normal curvatures are extremal and corresponding eigenvalues will be extremal curvatures. The extremal curvatures of the surface at a given point are called *principal curvatures* and denoted as ζ_1 and ζ_2. Using this it is useful to define the trace of the curvature tensor

$$\zeta = Tr(b_i^j) = g^{ij}b_{ij} = \zeta_1 + \zeta_2 \tag{A.23}$$

and the Gaussian curvature

$$\zeta_G = \det(b_i^j) = \zeta_1\zeta_2 \tag{A.24}$$

A.4 Surfaces with Translational Symmetry

If the surface possesses cylindrical symmetry, in a general case we can describe it by defining a two-dimensional curve and translating it along one of the axis. Then, the parameterization of the surface can be given in the following form

$$\vec{r}: \begin{cases} \mathbb{R}^2 \supset [-\infty;\infty] \times [a;b] & \to \mathbb{R}^3 \\ (y,t) & \mapsto \vec{r}(y,t) = \begin{pmatrix} x(t) \\ y \\ z(t) \end{pmatrix} \end{cases} \tag{A.25}$$

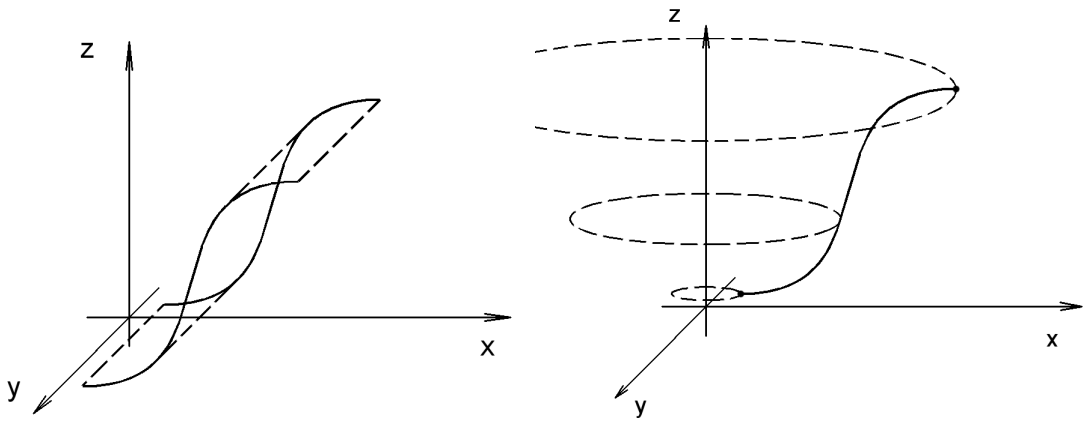

Figure A.2: Illustration of a parameterization of a translationally and rotationally symmetric surfaces

So here the surface is determined by two functions $x(t)$ and $z(t)$ which define a curve in the (x, z) plane. Then the translation is done along the y axis. Given the parameterization A.25 we can find the tangent vectors to be

$$\mathbf{e}_y = \frac{\partial \vec{r}}{\partial y} = \begin{pmatrix} 0 \\ 1 \\ 0 \end{pmatrix} \text{ and } \mathbf{e}_t = \frac{\partial \vec{r}}{\partial t} = \begin{pmatrix} \dot{x} \\ 0 \\ \dot{z} \end{pmatrix} \tag{A.26}$$

Given the tangent vectors we can construct the metric using the definition A.5

$$g_{ij} = \begin{pmatrix} 1 & 0 \\ 0 & \dot{x}^2 + \dot{z}^2 \end{pmatrix} \tag{A.27}$$

with the determinant

$$g = \dot{x}^2 + \dot{z}^2 \tag{A.28}$$

The inverse metric can be found to be

$$g^{ij} = \begin{pmatrix} 1 & 0 \\ 0 & 1/(\dot{x}^2 + \dot{z}^2) \end{pmatrix}. \tag{A.29}$$

By definition A.3 we can find the unit normal vector

$$\vec{n} = \frac{\mathbf{e}_y \times \mathbf{e}_t}{\sqrt{g}} = \frac{1}{\sqrt{\dot{x}^2 + \dot{z}^2}} \begin{pmatrix} \dot{z} \\ 0 \\ -\dot{x} \end{pmatrix}. \tag{A.30}$$

Therefore using A.17 we can obtain the second fundamental form

$$b_{ij} = \frac{1}{\sqrt{\dot{x}^2 + \dot{z}^2}} \begin{pmatrix} 0 & 0 \\ 0 & \ddot{x}\dot{z} - \ddot{z}\dot{x} \end{pmatrix}. \tag{A.31}$$

and its mixed version can be obtained by multiplying with with metric to raise one index.

$$b_i^j = b_{ik} g^{kj} = \frac{1}{\sqrt{\dot{x}^2 + \dot{z}^2}} \begin{pmatrix} 0 & 0 \\ 0 & \frac{\ddot{x}\dot{z} - \ddot{z}\dot{x}}{\dot{x}^2 + \dot{z}^2} \end{pmatrix}. \tag{A.32}$$

Eigenvalues and eigenvectors of this matrix can be found and we can obtain that two principal curvatures are

$$\kappa_1 = 0 \text{ and } \kappa_2 = \frac{\ddot{x}\dot{z} - \ddot{z}\dot{x}}{(\dot{x}^2 + \dot{z}^2)^{3/2}} \tag{A.33}$$

Eigenvectors are unit vectors along the coordinate lines, so principal directions are along $\mathbf{e}_y$ and $\mathbf{e}_t$. If we parameterize our curve $(x(t), z(t))$ by its arclength s, and describe the profile by specifying the angle of the tangent with respect to horizontal *psi* as a function of arclength s, we can use the following relations

$$\frac{dr}{ds} = \cos\psi \text{ and } \frac{dz}{ds} = \sin\psi. \tag{A.34}$$

These give us a relation

$$\dot{x}^2 + \dot{z}^2 = \cos\psi^2 + \sin\psi^2 = 1 \tag{A.35}$$

and simplify out expressions for curvatures into the following form

$$\kappa_1 = 0 \text{ and } \kappa_2 = -\dot{\psi} \tag{A.36}$$

A.5 Surfaces with Rotational Symmetry

The other case is when a system possesses rotational symmetry, it can be understood as a two-dimensional curve which is rotated around some axis (see Fig. A.2). The parameterization then will be

$$\vec{r}: \begin{cases} \mathbb{R}^2 \supset [0; 2\pi] \times [a; b] & \to \mathbb{R}^3 \\ (\phi, t) & \mapsto \vec{r}(\phi, t) = \begin{pmatrix} r(t)\cos\phi \\ r(t)\sin\phi \\ z(t) \end{pmatrix} \end{cases} \tag{A.37}$$

In this case, we have a plain curve defined by two functions $r(t)$ and $z(t)$, which is then rotated around the axis z. The tangent vectors then can be obtained

$$\mathbf{e}_\phi = \frac{\partial\vec{r}}{\partial\phi} = \begin{pmatrix} -r\sin\phi \\ r\cos\phi \\ 0 \end{pmatrix} \text{ and } \mathbf{e}_t = \frac{\partial\vec{r}}{\partial t} = \begin{pmatrix} \dot{r}\cos\phi \\ \dot{r}\sin\phi \\ \dot{z} \end{pmatrix} \tag{A.38}$$

We can construct the metric tensor in the same way

$$g_{ij} = \begin{pmatrix} r^2 & 0 \\ 0 & \dot{r}^2 + \dot{z}^2 \end{pmatrix}, \tag{A.39}$$

with a determinant

$$g = r^2(\dot{r}^2 + \dot{z}^2). \tag{A.40}$$

The inverse is then

$$g^{ij} = \frac{1}{r^2(\dot{r}^2+\dot{z}^2)}) \begin{pmatrix} \dot{r}^2+\dot{z}^2 & 0 \\ 0 & r^2 \end{pmatrix}. \tag{A.41}$$

The normal vector in this case is

$$\vec{n} = \frac{\mathbf{e}_\phi \times \mathbf{e}_t}{\sqrt{g}} = \frac{1}{\sqrt{\dot{r}^2+\dot{z}^2}} \begin{pmatrix} \dot{z}\cos\phi \\ \dot{z}\sin\phi \\ -\dot{r} \end{pmatrix}. \tag{A.42}$$

So the second fundamental form and it's mixed version can be obtained

$$b_{ij} = \frac{1}{\sqrt{\dot{r}^2+\dot{z}^2}} \begin{pmatrix} -r\dot{z} & 0 \\ 0 & \ddot{r}\dot{z}-\ddot{z}\dot{r} \end{pmatrix} \tag{A.43}$$

$$b_i^j = b_{ik}g^{kj} = \frac{1}{\sqrt{\dot{r}^2+\dot{z}^2}} \begin{pmatrix} -\frac{\dot{z}}{r} & 0 \\ 0 & \frac{\ddot{r}\dot{z}-\ddot{z}\dot{r}}{\dot{x}^2+\dot{z}^2} \end{pmatrix}. \tag{A.44}$$

The eigenvalues of b_i^j will be the principal curvatures

$$\kappa_1 = -\frac{\dot{z}}{r\sqrt{\dot{r}^2+\dot{z}^2}} \text{ and } \kappa_2 = \frac{\ddot{r}\dot{z}-\ddot{z}\dot{r}}{(\dot{r}^2+\dot{z}^2)^{3/2}} \tag{A.45}$$

Using the arclength parameterization exactly as in the case for translational symmetry we can represent our curvatures in the following form

$$\kappa_1 = -\frac{\sin\psi}{r} \text{ and } \kappa_2 = -\dot{\psi}. \tag{A.46}$$

References

[1] Robert B. Gennis. *Biomembranes - Molecular Structure and Function*. Springer-Verlag, 1989. 1, 3

[2] Markus Deserno. Fluid lipid membranes - a primer. 2

[3] Martin Michael Muller. *Theoretical Studies of Fluid Membrane Mechanics*. 2007. 2

[4] Harwey Lodish, Arnold Berk, Lawrence S. Zipursky, Paul Matsudaira, David Baltimore, and James Darnell. *Molecular Cell Biology*. W. H. Freeman and Company, 4 edition, 2000. 2

[5] Markus Deserno and William M. Gelbart. Adhesion and wrapping in colloid-vesicle complexes. *Journal of Physical Chemistry B*, 106:5543–5552, 2002. 3

[6] Sung S. Rhee, Huxiong Hui, , and Eric Hunter. Preassembled capsids of type d retroviruses contain a signal sufficient for targeting specifically to the plasma membrane. *Journal of Virology*, 64(8):3844–3852, 1990. 3

[7] Henrik Garoff, Roger Hewson, and Dirk-Jan. E. Opstelten. Virus maturation by budding. *Microbiology and Molecular Biology Reviews*, 62(4):1171–1190, 1998. 3, 7

[8] O. Boussif, F. Lezoualc'h, M. A. Zanta, M. D. Mergny, D. Scherman, B. Demeneix, W. Helfrich, and J. P. Behr. A versatile vector for gene and oligonucleotide transfer into cells in culture and in vivo: polyethylenimine. *Proceedings of the National Academy of Sciences of the United States of America*, 92(16):7297–7301, 1995. 3

[9] Robert M. Hochmuth, Jin-Yu Shao, Jianwu Dai, and Michael P. Sheetzt. Deformation and flow of membrane into tethers extracted from neuronal growth cones. *Biophysical Journal*, 70:358–369, 1996. 3

[10] Robert M. Henderson and Hans Oberleithner. Pushing, pulling, dragging, and vibrating renal epithelia by using atomic force microscopy. *Am. J. Physiol. Renal. Physiol.*, 278(5):F689–F701, 2000. 3

[11] Danilo D. Lasic. *Medical Applications Of Liposomes*. Elsevier, 1998. 4

[12] R. Lipowsky and H.-G. Dobereiner. Vesicles in contact with nanoparticles and colloids. *Europhysics Letters*, 43:219–225, 1998. 4

[13] Hiroshi Noguchi and Masako Takasu. Adhesion of nanoparticles to vesicles: A brownian dynamics simulation. *Biophysical Journal*, 83:299–308, 2002. 4

[14] Ilya Koltover, Joachim O. Radler, and Cyrus R. Safinya. Membrane mediated attraction and ordered aggregation of colloidal particles bound to giant phospholipid vesicles. *Physical Review Letters*, 82:1991 – 1994, 1999. 4

[15] Yang Li, Xin Chen, and Ning Gu. Computational investigation of interaction between nanoparticles and membranes: Hydrophobic/hydrophilic effect. *The Journal of Physical Chemistry B*, 112(51):16647–16653, 2008. 4

[16] Wolfgang H. Binder, Robert Sachsenhofer, Dominique Farnika, and Dieter Blaasb. Guiding the location of nanoparticles into vesicular structures: A morphological study. *Physical Chemistry Chemical Reviews*, 9:6435–6441, 2007. 4

[17] Udo Seifert. Configurations of fluid membranes and vesicles. *Advances in Physics*, 46(1):13–137, 1997. 4

[18] A. Boulbitch. Enforced unbinding of a bead adhering to a biomembrane by generic forces. *Europhysics Letters*, 59(6):910, 2002. 4, 6, 19

[19] Thomas R. Weikl. Indirect interactions of membrane-adsorbed cylinders. *European Physics Journal E*, 12:265–273, 2003. 4, 6, 24

[20] Markus Deserno. Elastic deformation of a fluid membrane upon colloid binding. *Physical Review Letters E*, 69:031903, 2004. 5, 11, 19, 20

[21] Martin Michael Muller and Markus Deserno. Balancing torques in membrane-mediated interactions: Exact results and numerical illustrations. *Physical Review E*, 76:011921, 2007. 5, 6, 26

[22] C. E. Morris and U. Homann. Cell surface area regulation and membrane tension. *The Journal of Membrane Biology*, 179:79–102, 2001. 7

[23] W. Helfrich. Elastic properties of lipid bilayers: theory and possible experiments. *Z Naturforsch [C]*, 28:693, 1973. 11

[24] Jeff Z.Y. Chen, Y. Liu, and H.-J. Liang. Structure of a tubular membrane confining spherical particles. 24

[25] Yaron R. Silberberg, Andrew E. Pelling, Gleb E. Yakubov, William R. Crum, David J. Hawkes, and Mike A. Horton. Tracking displacements of intracellular organelles in response to nanomechanical forces. *Biomedical Imaging: From Nano to Macro*, pages 1335–1338, 2008. 37

[26] Markus Deserno. Notes on differential geometry. 47

[27] Andrew Pressley. *Elementary Differential Geometry*. Springer, 2005.

[28] Udo Seifert, Karin Berndl, and Reinhard Lipowsky. Shape transformations of vesicles: Phase diagram for spontaneous curvature and bilayer-coupling models. *Physical Review A*, 44(2):1182–1202, 1991.

[29] Frank Julicher and Udo Seifert. Shape equations for axissymmetric vesicles: A clarification. *Physical Review E*, 49(5):4728–4731, 1994.

[30] Markus Deserno. When do fluid membranes engulf sticky colloids? *Journal of Physics: Condensed Matter*, 16:S2061–S2070, 2004.

[31] Yanping E. Lu and Margaret Kielian. Semliki forest virus budding: Assay, mechanisms, and cholesterol requirement. *Journal of Virology*, 74(17):7708–7719, 2000.

[32] Jeff Z.Y. Chen. Swollen-to-globular transition of a self-avoiding polymer confined in a soft tube. *Physical Review Letters*, 98:088302, 2007.

[33] Avi Caspi, Orna Yeger, Inna Grosheva, Alexander D. Bershadsky, and Michael Elbaum. A new dimension in retrograde flow: Centripetal movement of engulfed particles. *Biophysical Journal*, 81(4):1990–2000, 2001.

[34] Benedict J. Reynwar, Gregoria Illya, Vagelis A. Harmandaris, Martin M. Muller, Kurt Kremer, and Markus Deserno. Aggregation and vesiculation of membrane proteins by curvature-mediated interactions. *Nature*, 447:461–464, 2007.